CAPITAL UNIVERSITY OF SCIENCE AND
TECHNOLOGY, ISLAMABAD

Mode Filtering using Permeable Membrane Cavity

by

Aasia Bibi

A thesis submitted in partial fulfillment for the
degree of Master of Philosophy

in the

Faculty of Computing
Department of Mathematics

2025

I dedicate my thesis to

my beloved family, friends specially

My Mother in law,

A determined and aristocratic embodiment who educate me to belief in ALLAH,

believe in hard work and that so much could be done with little,

My Father in law

I quote the remarkable words of Hadith,

"A father gives his child nothing better than an education."

CERTIFICATE OF APPROVAL

Mode Filtering using Permeable Membrane Cavity

by

Aasia Bibi

(Registration No: MMT231017)

THESIS EXAMINING COMMITTEE

S. No.	Examiner	Name	Organization
(a)	External Examiner	Dr. Amer Bilal Mann	FUUAST, Islamabad
(b)	Internal Examiner	Dr. Samina Batul	CUST, Islamabad
(c)	Supervisor	Dr. Muhammad Afzal	CUST, Islamabad

Dr. Muhammad Afzal
Thesis Supervisor
April, 2025

Dr. Muhammad Sagheer
Head
Dept. of Mathematics
April, 2025

Dr. Muhammad Abdul Qadir
Dean
Faculty of Computing
April, 2025

Author's Declaration

I, **Aasia Bibi** hereby state that my MPhil thesis titled "**Mode Filtering using Permeable Membrane Cavity**" is my own work and has not been submitted previously by me for taking any degree from Capital University of Science and Technology, Islamabad or anywhere else in the country/abroad.

At any time if my statement is found to be incorrect even after my graduation, the University has the right to withdraw my MPhil Degree.

(Aasia Bibi)

Registration No: MMT231017

Plagiarism Undertaking

I solemnly declare that the research work presented in this thesis titled "**Mode Filtering using Permeable Membrane Cavity**" is solely my research work with no significant contribution from any other person. The small contribution/help wherever taken has been duly acknowledged and that complete thesis has been written by me.

I understand the zero tolerance policy of the HEC and Capital University of Science and Technology towards plagiarism. Therefore, as an author of the above titled thesis, I declare that no portion of my thesis has been plagiarized and any material used as reference is properly referred/cited.

I undertake that if I am found guilty of any formal plagiarism in the above titled thesis even after award of MPhil Degree, the University reserves the right to withdraw/revoke my MPhil degree and that HEC and the University have the right to publish my name on the HEC/University website on which names of students are placed who submitted plagiarized work.

(Aasia Bibi)

Registration No: MMT231017

Acknowledgement

In the name of **ALLAH**, who is the most merciful and beneficent, created the universe and blessed the mankind with intelligence and wisdom to explore its secret. I would like to express my heart felt gratitude and immeasurable respect to my supervisor **Dr. Muhammad Afzal** for his passionate interest, willingness help, superb guidance and inspiration throughout this investigation. His textural and verbal criticism enabled me in formatting this thesis.

I am extremely grateful to my all teachers for their encouragement and emphasis on striving for excellence when teaching mathematics. I would like to acknowledge the CUST for providing me such a favourable environment to this research.

I must express my very profound gratitude to my dear parents and whole members of my family including my Husband **Aamir Iqbal** and my beloved Daughters **Anabiya**, **Arooshay Isma**, **Anaysha Irum** for providing me with unfailing support and continuous encouragement throughout my years of study and through the process of researching and writing this thesis.

Finally, I want to express my gratitude to my Friends who encouraged me throughout my MPhil research. I am grateful to my fellow researchers at CUST for valuable discussions on this research. I have enjoyed working alongside them in a pleasant working environment.

(Aasia Bibi)

Registration No: MMT231017

Abstract

This thesis presents an analytical study on the propagation and scattering of acoustic waves in cylindrical waveguides with tensioned, permeable membranes. The research aims to understand the impact of these membranes on wave behavior, particularly in terms of reflection, transmission, and mode filtering. A mode-matching technique is employed to develop mathematical models that describe the acoustic interactions at membrane interfaces. The study investigates different configurations, including rigid and soft cavities, to assess the influence of boundary conditions on wave propagation. The results demonstrate that membrane properties, such as tension and permeability, play a crucial role in shaping acoustic wave transmission and scattering.

Contents

List of Figures

Abbreviations

BEM	Boundary Element Method
BVPs	Boundary Value Problems
FEM	Finite Element Method
MMT	Mode Matching Technique
OR	Orthogonality Relation
SL	Sturm Liouville

Symbols

a	Non-dimensional radius of duct I and II
c	Speed of sound
c_m	Speed of wave on membrane
T	Membrane tension
ρ_m	Membrane mass density
ρ	Density of fluid
α	Fluid loading parameter
μ	Membrane wave number capacitance
k	Wave number
ω	Non-dimensional displacement
μ	Flow velocity
g	Gravitational acceleration
∇p	Exerting forces
ρg	Body forces
γ	Specific gas constant
C_p	Specific heat at constant pressure
C_v	Specific heat at constant volume
Z	Impedance of surface

Chapter 1

Introduction

Acoustics plays a vital role in understanding and managing sound behavior in various environments, ranging from industrial noise control to architectural acoustics. Among the many tools and materials used in noise control engineering, tensioned, permeable membranes have emerged as highly versatile elements for managing sound propagation, transmission, and attenuation. A tensioned, permeable membrane is a thin, flexible structure under mechanical tension that allows partial passage of sound waves while interacting with them through vibration, absorption, or redirection. These membranes find applications in diverse fields, such as sound barriers, acoustic filters, and resonators, due to their ability to alter acoustic wave behavior selectively.

The performance of such membranes depends on various factors, including material properties, tension levels, and permeability characteristics. Permeability refers to the ability of the membrane to transmit air or sound energy, which is governed by the size, distribution, and structure of pores within the material. The interaction between these properties and the acoustic environment necessitates sophisticated modeling approaches to predict and optimize membrane behavior effectively. In acoustics, boundaries play a crucial role in shaping wave propagation. A rigid boundary, for instance, is defined as a surface that does not support vibration and reflects sound entirely, with its normal velocity being zero. For tensioned, permeable membranes, however, the boundary conditions are more complex, involving impedance and vibrational responses influenced by tension and material permeability.

This thesis focuses on the acoustical modeling of tensioned, permeable membranes to gain a deeper understanding of their behavior in the context of noise control engineering. The primary objective is to develop mathematical models that accurately characterize the acoustic interactions involving these membranes, capturing the complex dynamics introduced by both tension and permeability. In addition, the study investigates a range of boundary conditions, including rigid and impedance-based formulations, to better reflect the diversity of real-world applications. To ensure the reliability and practical relevance of the models, they are validated against experimental data and evaluated for their performance in realistic noise control scenarios. Through this research, the aim is to contribute to the development and optimization of effective noise mitigation solutions that exploit the distinctive properties of tensioned, permeable membranes. The outcomes of this work are expected to enhance acoustic performance in various applications, including industrial facilities, architectural designs, and environmental noise management systems

Tensioned permeable membranes are utilized extensively across engineering and architectural disciplines due to their distinctive acoustic, mechanical, and structural characteristics. The Mode Matching Technique (MMT) proves especially effective for analyzing these membranes, as it incorporates the effects of membrane tension and vibrational response, which significantly alter the local acoustic field. By implementing impedance-based boundary conditions, MMT accurately models partial sound transmission through the membrane, capturing the complex interactions among incident, reflected, and transmitted waves that arise at acoustic discontinuities. These properties make tensioned permeable membranes ideal for sound control applications. In architectural acoustics, they are commonly integrated into buildings and concert halls to regulate sound transmission and enhance absorption. Ma et al. [1] highlighted their capacity to dissipate sound energy, making them effective for reducing noise pollution in both indoor and outdoor environments. Sun et al. [2] further demonstrated their acoustic advantages by incorporating them into lightweight roofing systems and façade elements to enhance acoustic comfort. In the aerospace sector, these membranes have been applied in aircraft cabins and engine nacelles to mitigate noise produced by jet engines and aerodynamic flow, offering improved passenger comfort without compromising structural weight efficiency.

Toyoda et al. [3] explored the use of tensioned membranes in industrial acoustics, where they were integrated into noise barriers, enclosures, and ventilation ducts to absorb and dissipate sound energy. In manufacturing and processing environments, these membranes have been applied to mitigate machinery and ventilation noise, thereby improving workplace safety and ensuring compliance with regulatory noise limits.

Hao et al. [4] demonstrated the application of permeable membranes in environmental acoustics, particularly in outdoor noise control along highways, railways, and urban settings. These membranes have been employed in noise barriers to reduce the impact of traffic-related noise, contributing to improved urban soundscapes and promoting sustainable city planning. Wang et al. [5] investigated the use of tensioned membranes in medical and laboratory contexts, where they were incorporated into diagnostic devices, air filtration systems, and bioacoustic research tools. In biomedical engineering, these membranes offer enhanced acoustic permeability and selective transmission, enabling more accurate diagnostics and improved research outcomes.

1.1 Literature Review

The foundational work of Strutt and Rayleigh [6] laid the groundwork for modern noise control engineering. Their "Theory of Sound" introduced key concepts related to sound propagation, reflection, absorption, and transmission. These principles have since been expanded through computational methods such as the Finite Element Method (FEM) and Boundary Element Method (BEM), as highlighted by Kirkup [7], allowing for the simulation of complex acoustic environments. The role of acoustical modeling in noise control has been widely studied. Mak and Wang [8], for instance, used FEM to analyze acoustic barriers, emphasizing the importance of boundary conditions in accurately predicting sound attenuation. However, traditional models often assume rigid or fully absorptive boundaries, overlooking the dynamic behavior of flexible membranes. Zhang et al. [9] examined the acoustic properties of microperforated membranes, evaluating their effectiveness in sound absorption based on pore size and distribution. Similarly, Pierce [10] studied the impedance of porous materials, offering insights into energy dissipation mechanisms and their impact on acoustic

performance. These investigations have advanced our understanding of how porous structures influence sound attenuation.

Despite significant progress, much of the existing research has focused on static membranes. Lannoy et al. [11] explored the vibrational dynamics of tensioned membranes, analyzing how tension affects vibrational modes. However, the acoustic interaction of vibrating permeable membranes remains insufficiently explored. Mo et al. [12] investigated classical boundary conditions, such as the rigid-wall condition $\hat{\mathbf{n}}.\Delta\Phi = 0$, which are critical in computational acoustics for defining wave-surface interactions. In contrast, permeable membranes require boundary conditions that incorporate both structural vibrations and energy transmission effects. Advances in acoustic materials have been demonstrated by Wang and Craster [13], who developed hyper-thin acoustic metasurfaces using membrane resonators. These metasurfaces enable subwavelength manipulation of sound waves, offering precise control over pressure fields and paving the way for next-generation acoustic devices.

While the mode-matching technique is a robust tool for solving boundary value problems involving horizontal membranes or elastic plates with various boundary conditions, it is less effective for cases involving vertical or bridging membranes. This challenge was addressed by McAlpine and Fisher [14]. Additionally, Takahashi et al. [15] developed a theoretical framework to analyze sound absorption and transmission through permeable membranes in building materials, validating the model against experimental results and confirming its predictive reliability. Mode matching continues to be a powerful method for analyzing acoustic wave interactions in complex media. It has been especially effective in modeling membrane-based systems for noise control in structures with geometric discontinuities, multilayered compositions, or flexible boundaries. Its utility in predicting wave behavior and transmission loss is evident in several recent studies [16–26].

The acoustic behavior of tensioned permeable membranes is fundamentally based on classical membrane vibration theory. Traditional models predominantly focused on impermeable membranes, often neglecting the effects of acoustic permeability. Foundational work by Morse and Ingard [27] established a theoretical basis for sound propagation and its interaction with thin, flexible structures. However, these early models

did not consider the impact of airflow resistivity or the interaction of sound waves with permeable surfaces. To address this limitation, Cao et al. [28] developed a theoretical framework for analyzing sound absorption and transmission through single permeable membranes. Their findings illustrated how acoustic permeability, in combination with membrane tension, influences transmission loss and absorption characteristics. Building on this work, Mechel and others expanded the theory to include multilayered configurations incorporating absorptive materials and air gaps, thereby enhancing the accuracy of acoustic performance predictions in complex systems. Allard and Atalla [29] contributed valuable experimental data on airflow resistivity and its influence on sound absorption. Their study emphasized the critical role of membrane porosity and surface tension in governing acoustic behavior. In a related effort, Wu et al. conducted comparative analyses between theoretical predictions and experimental measurements for membranes with varying permeability and tension, revealing the significance of boundary conditions and membrane thickness in shaping acoustic responses.

Kang et al. [30] explored how airflow resistivity interacts with surface tension under varying environmental conditions, such as humidity and temperature. Their work underscored the importance of adaptive modeling techniques to accurately capture dynamic environmental effects on acoustic performance. Further insight into acoustic radiation was provided by Kang and Bolton [31], who modeled the sound radiation from a rolling tire. Their study incorporated tire surface vibrations and the effects of acoustic cavity modes, demonstrating how deformation and Doppler effects influence the interaction between cavity resonances and structural treadband modes. This work is particularly relevant in automotive noise control, where finite element models were employed to predict structural vibration and boundary element methods used to evaluate sound radiation, including ground surface interactions.

Song [32] investigated non-fibrous acoustic materials, such as glass bubbles, which exhibit level-dependent behavior. At low excitation levels, these materials behave solid-like, whereas at higher levels they show fluid-like characteristics. In contrast, conventional absorptive materials—such as fibrous webs and foams—are typically modeled as level-independent equivalent fluids. Song proposed a two-dimensional finite difference model based on Biot's poroelastic theory, capable of capturing the level-dependent

behavior of granular materials. Brambley and Peake [33] further examined the classification of surface acoustic modes and highlighted the necessity of accounting for viscous effects and boundary layers in the presence of flow. Wang and Mak [34] studied wave propagation in ducts lined with periodic resonators, while Abbas et al. [35] analyzed wave dissipation in discontinuous flexible waveguides. Lawrie and Abrahams [36] contributed a deeper theoretical understanding by exploring generalized orthogonality in boundary value problems with higher-order boundary conditions. Despite its computational intensity, the mode-matching technique remains a cornerstone in the analysis of wave propagation and field behavior. Its precision and adaptability have enabled researchers to model complex boundary and interface problems with high accuracy, as demonstrated across a wide range of studies [37–48].

In a related development, Huang and Zhang [49] proposed an efficient mode-matching method for analyzing axisymmetric coaxial discontinuities. Their method achieved high accuracy in computing S-parameters and field distributions, and the results closely aligned with established techniques. Afzal et al. [50] addressed waveguide scattering in flexible structures using a mode-matching approach grounded in orthogonality principles. This study examined wave reflection and transmission across discontinuities caused by abrupt geometric and material changes, presenting numerical validation and a detailed discussion of energy flux and power conservation. Meylan and Bashir [51] extended the mode-matching method to solve trifurcated and pentafurcated waveguide problems. Their work validated the approach by revisiting classical problems previously addressed using the Wiener–Hopf technique, demonstrating that mode matching is not only simpler to implement but also more versatile. The numerical solutions provided valuable insights into practical waveguide geometries, such as those found in exhaust systems.

Originally designed for canonical problems involving the Laplace or Helmholtz equations with Dirichlet, Neumann, or Robin boundary conditions, mode matching has evolved to accommodate increasingly complex geometries and boundary types. Lawrie and Afzal [45] applied this technique to study wave reflection and transmission at discontinuities in ducts and pipes. Their work reinforced the utility of mode matching in acoustical engineering, particularly for analyzing sound-wave behavior at complex interfaces. These boundary value problems are often governed by Helmholtz and

Laplace equations and require advanced treatment of rigid, soft, or impedance conditions. Although early models idealized boundaries as perfectly clamped, real-world applications often involve elastic or partially constrained supports. Mode matching has proven capable of handling such realistic scenarios, as shown in a series of recent investigations [52–64].

The primary objective of this study is to develop mathematical models that accurately capture the interaction of sound waves with tensioned, permeable membranes. A particular focus is placed on understanding how various boundary conditions—such as rigid and soft cavities—affect wave propagation characteristics. The study also investigates the influence of membrane properties, including tension and permeability, on wave transmission and scattering phenomena. To analyze wave behavior at discontinuities within waveguides, the Mode Matching Technique (MMT) is employed. Furthermore, theoretical predictions are validated through numerical simulations, with an emphasis on their practical relevance to real-world noise control applications.

This research offers meaningful contributions to the understanding of acoustic wave behavior in waveguide systems. It establishes a robust mathematical framework for analyzing wave propagation and membrane interactions in cylindrical waveguides with permeable boundaries. By exploring a range of boundary conditions—including rigid and impedance-based types—the study provides insights into optimizing acoustic filtering performance. Computational results, obtained through numerical simulations, serve to validate the theoretical models and illustrate the behavior of wave modes across different frequency ranges. Additionally, an advanced mode-filtering technique is introduced, enabling controlled and selective wave transmission, with potential applications in acoustic engineering and waveguide design.

1.2 Thesis Structure

The structure of the thesis is as follows:

- **Chapter 2** introduces some preliminaries concepts and definitions that are useful in understanding the work presented in rest of the chapters.

- **Chapter 3** presents the theoretical framework for acoustical modeling including the governing equations for incident and transmitted sound waves as well as membrane vibrations. It defines the boundary conditions, ensuring continuity of velocity and force equilibrium across the membrane. In addition, it formulates sound power calculations that cover incident, transmitted and dissipated power components.

- **Chapter 4** explores acoustic wave propagation and scattering of acoustic waves in membranes near rigid boundaries, focusing on two cases: a membrane in a rigid cavity and a permeable membrane backed by a soft cavity. This chapter cover mathematical modeling for both cases and presents computational results and discussion.

- **Chapter 5** presents the final remarks of the study.

Finally, references cited throughout the thesis are listed in the bibliography.

Chapter 2

Preliminaries

This chapter depicts the fundamental concepts that are relevant to understand the propagation and scattering of acoustic wave in waveguides. The acoustic cavity problem are governed with different types of boundary conditions. The boundary conditions is considered to be rigid, spring like, and fixed. The physical problem are governed by Helmholtz's and having boundary condition rigid and the governing eigenfunction satisfy the orthogonality condition.

2.1 Acoustic

The word "acoustics" comes from the Greek word akouein, meaning "to hear." In 1701, Sauveur was the first to use the term "acoustics" to describe the science of sound. Initially, acoustics focused on studying small pressure or compression waves that the human ear could detect. Over time, the field expanded to include both infrasound (low-frequency sound) and ultrasound (high-frequency sound).

Today, acoustics is a branch of physics that studies mechanical vibrations without any frequency limitations. It has numerous subfields, such as structural acoustics, physical acoustics, engineering acoustics, bioacoustics, environmental acoustics, musical acoustics and architectural acoustics.

2.2 Acoustic Setting

Acoustic waves are the pressure fluctuations in a material medium which transfer energy from one point to another point of medium. The medium can be solid, liquid, and gases.

The equation of motion responsible for the propagation of acoustic waves in such a medium can be derived by considering the conservation law and thermodynamic properties of the medium.

2.3 Acoustic Wave Equation

The linear acoustic wave equation defines the propagation of pressure perturbations in the fluid medium. The movement of sound waves can be described by a differential equation, which depends on the properties of the medium whether solid, liquid, or gas through which the sound propagates. This equation is grounded in fundamental conservation laws, including the conservation of mass, momentum and energy. In this context we aim to derive the wave equation specifically for gases like air. Although the conservation laws and resulting wave equation are generally nonlinear, solving the nonlinear form can be complex. To simplify the analysis, the linear approximation is commonly applied, as it is more manageable and practical in many situations. In this discussion, we focus on deriving the wave equation in its linear form.

2.3.1 Conservation of Mass

The conservation of mass equation states that the sum of the net mass flow per unit time and the instantaneous rate of change of mass density is zero.

This is expressed as:

$$\frac{\partial \rho}{\partial t} + \nabla.(\rho u) = 0, \tag{2.1}$$

where u represents the flow velocity and ρ denotes the instantaneous mass density.

2.3.2 Conservation of Momentum

The conservation of momentum equation connects the net momentum per unit volume and time to the forces acting upon it expressed as:

$$\frac{\partial(\rho u)}{\partial t} = -\nabla.(\rho u)u - \nabla p + \rho g, \tag{2.2}$$

where p represents pressure, g is the gravitational acceleration, ∇_p denotes exerting forces and ρg represent the body forces. By using equation (2.1), we can write

$$\rho\frac{Du}{Dt} = -\nabla p + \rho g, \tag{2.3}$$

where $\dfrac{D}{Dt} = \dfrac{\partial}{\partial t} + u.\nabla$ is the total derivative. The first term represents the time derivative, and the second term accounts for convection.

2.3.3 Equation of State for a Perfect Gas

The thermodynamic behavior of a compressible fluid is described by the equation of state. For a perfect gas, it is given as:

$$p = \rho r T, \tag{2.4}$$

where,

- p is the pressure,
- ρ is the density,
- T is the temperature,
- r is the specific gas constant.

Isothermal condition for a gas confined within a vessel with highly thermally conductive walls, the process can be considered isothermal. The isothermal condition is

expressed as:

$$\frac{p}{p_0} = \frac{\rho}{\rho_0}, \tag{2.5}$$

where p_0 and ρ_0 are the static pressure and density, respectively.

In an adiabatic process, where no heat is exchanged with the surroundings the relationship between pressure and density is given by:

$$\frac{p}{p_0} = \left(\frac{\rho}{\rho_0}\right)^{\gamma}, \tag{2.6}$$

where, γ is the adiabatic index, defined as the ratio of specific heats;

$$\gamma = \frac{C_p}{C_v},$$

here, C_p and C_v are the specific heats at constant pressure and constant volume, respectively.

The change in density relative to the static density is described by the acoustic condensation, s

$$s = \frac{\rho - \rho_0}{\rho_0}, \tag{2.7}$$

which implies

$$\rho = \rho(1 + s). \tag{2.8}$$

Substituting this into the adiabatic condition, (2.6) gives:

$$\frac{p}{p_0} = (1 + s)^{\gamma}. \tag{2.9}$$

For small perturbations ($s << 1$), expanding the equation using the binomial series yield

$$\frac{p}{p_0} \approx 1 + \gamma s, \tag{2.10}$$

or equivalently:

$$p - p_0 = \gamma p_0 s. \tag{2.11}$$

The pressure can also be expressed as a Taylor expansion around the static density, ρ_0

$$p \approx (\rho_0) + \frac{\partial p}{\partial \rho} \mid_{\rho=\rho_0} (\rho - \rho_0). \tag{2.12}$$

Using the relationship for acoustic condensation, (2.11) the above simplifies to:

$$\frac{\partial p}{\partial \rho} \mid_{\rho=\rho_0} (\rho - \rho_0) = \gamma p_0 s. \tag{2.13}$$

Equating this with the earlier expression for $(p - p_0)$ we find;

$$\gamma = \frac{\beta}{p_0}, \tag{2.14}$$

where

$$\beta = \rho_0 \frac{\partial p}{\partial \rho} \mid_{\rho=\rho_0} .$$

The pressure fluctuation, or acoustic pressure P, is defined as

$$P = p - p_0 = \beta s. \tag{2.15}$$

The continuity equation (2.1) can be linearized as

$$\frac{\partial s}{\partial t} + \nabla . u = 0. \tag{2.16}$$

Here we use the acoustic density $\rho = \rho_0(1 + s)$. The Euler equation of motion of small amplitudes pressure fluctuations is given

$$\rho_0 \frac{\partial u}{\partial t} = -\nabla P. \tag{2.17}$$

Taking the divergence of (2.17):

$$\frac{\partial}{\partial t}(\nabla . u) = -c\nabla^2 P. \tag{2.18}$$

By differentiating (2.16) with respect to t, we obtain

$$\frac{\partial}{\partial t}(\nabla . \mathbf{u}) = -\frac{\partial^2 s}{\partial t^2}. \tag{2.19}$$

From equation (2.18) and (2.19) we obtain

$$\frac{\partial^2 s}{\partial t^2} = \frac{1}{\rho_0} \nabla^2 P. \tag{2.20}$$

Using, $\nabla^2 P = \frac{1}{c^2}\frac{\partial^2 P}{\partial t^2}$ where, $c^2 = \frac{\beta}{\rho_0}$, gives

$$\nabla^2 P = \frac{1}{c^2}\frac{\partial^2 P}{\partial t^2}. \tag{2.21}$$

Equation (2.21) is known as acoustic wave equation in term of pressure.
Throughout this dissertation, we are looking for steady harmonic solutions. It is useful to develop the wave, membrane, and displacement equations in the above mentioned form. For this purpose we assume that $\tilde{P}(r,z,t) = P(r,z)e^{-i\omega t}$, $\tilde{Y}(r,t) = Y(r)e^{-i\omega t}$ and $\tilde{U}(r,t) = U(r)e^{-i\omega t}$ where ω is the radian frequency, using the above substitution in the wave equation (2.21), we obtained

$$\left\{\frac{\partial^2}{\partial r^2} + \frac{1}{r}\frac{\partial}{\partial r} + \frac{\partial^2}{\partial z^2} + k^2\right\} P = 0. \tag{2.22}$$

The equation (2.22) is known as Helmholtz's equation.

2.4 Membrane

In acoustic waveguides, a membrane refers to a thin plate or diaphragm that vibrates in response to sound waves, influencing wave propagation.

Membranes serve various purposes, such as

- Separation of different sections of the waveguide
- Introducing discontinuities or obstacles
- Enhancing or suppressing specific frequency ranges
- Acting as filters or resonators

These membranes are essential in shaping wave behavior, including scattering and transmission, within the waveguide.

2.4.1 Permeable Membrane

Permeable membrane refers to a thin flexible material under mechanical tension that allows the controlled passage of air or sound waves. These membranes are designed to interact with sound waves by attenuating, filtering, or transmitting them selectively, depending on their material properties and structural configuration.

Such membranes are often used in noise control engineering to manage sound transmission and absorption in environments such as industrial facilities, concert halls, or urban spaces.

2.5 Boundary Conditions

The boundary conditions play an important role in determining the mathematical solutions to physical problems. The nature and types of boundary conditions depend on the conditions assumed while modeling the physical problems.

2.5.1 Soft Conditions

The soft boundary conditions are Drichlet's type boundary conditions. In these type of conditions, the pressure or displacement is consider as zero, i.e.

$$\phi(x, y) = 0.$$

2.5.2 Rigid Conditions

Neumann's type boundary conditions are actually rigid boundary conditions. In rigid conditions, normal velocity is consider as zero, i.e.

$$\frac{\partial \phi}{\partial x} = 0.$$

Here the equation is Neumann type boundary condition specifies a directional derivative of a function along the outward normal to the boundary.

2.5.3 Edge Conditions

Edge conditions in a waveguide are the boundaries or constraints imposed on the wavefield at the edges, determining how the wave behaves such as reflection, absorption, or transmission. Common edge conditions include hard wall, soft wall, periodic, absorbing, and impedance boundaries.

2.5.4 Spring-like Conditions

Spring-like conditions in a waveguide or acoustic system are boundaries that:

- Allow displacement in response to force (pressure)
- Return to their original position when the force is removed

2.5.5 Fixed Conditions

In a waveguide, a fixed condition, also known as a "fixed boundary" or "clamped boundary", is a boundary where:

- The displacement (movement) is zero

$$u = 0, v = 0, w = 0.$$

- No slop

$$\frac{\partial u}{\partial z} = 0, \frac{\partial v}{\partial z} = 0, \frac{\partial w}{\partial z} = 0.$$

- The wavefield is not allowed to move or vibrate
- The boundary is rigid and immovable

These conditions ensure the edges are fully constrained with no motion or rotation.

2.5.6 Free Conditions

In a waveguide, a free condition, also known as a "free boundary" or "unbounded boundary", is a boundary where:

- The wavefield is allowed to move or vibrate freely
- There are no constraints on the displacement (movement)
- The boundary is not rigid or fixed

2.5.7 Rigid Boundary Condition

In acoustics, a rigid boundary is defined as a surface that remains stationary and does not vibrate or deform when exposed to incident sound waves. A surface is considered acoustically rigid when $z \to \infty$, and that reveals from (2.21), that can be written as

$$\hat{\mathbf{n}}.V = 0 \quad on \quad \Omega, \tag{2.23}$$

where, the boundary is represented by Ω and $\hat{\mathbf{n}}$ denotes the outward normal vector to boundary Ω. The rigid boundary conditions using harmonic time dependance can be expressed as

$$\frac{\partial p}{\partial r} = 0, \quad r = 0. \tag{2.24}$$

2.6 Orthogonality Relations

This thesis addresses physical problems using matching techniques. These methods involve representing field potentials through eigenfunction expansions and applying the orthogonal properties of the corresponding eigensubsystems.

For problems described by Helmholtz's equation with boundary conditions such as Dirichlet, Neumann, or Robin types, the eigenfunctions fall into the category Sturm-Liouville (SL) and satisfy standard orthogonality rules.

For tensioned, permeable membranes, acoustic modes can be represented as solutions to the governing wave equation with specific boundary conditions. Let $R_n(r)$ and $R_m(r)$ represent two different modes (eigenfunctions). The orthogonality condition is expressed as:

$$\int_0^a R_n(r)R_m(r)rdr = 0 \quad for \quad m \neq n. \tag{2.25}$$

2.7 Mode Matching Technique

Modal representation is commonly used to solve acoustic waveguide problems. However, a single modal representation can only be applied in sections of a duct where properties such as diameter and wall impedance remain constant. When two segments with different characteristics are connected, each segment requires its own modal representation. Since the modes in each segment differ, the incident field must be reformulated into an expansion of the transmitted field in the adjacent segment while ensuring the continuity of pressure and velocity. The mode matching technique is a cornerstone in the acoustical modeling of tensioned, permeable membranes. Its ability to handle complex boundary interactions and discontinuities makes it indispensable for predicting and optimizing noise control solutions involving such structures. This structure presents the technique clearly, connects it to the topic of tensioned, permeable membranes, and highlights its relevance and advantages. This approach is known as the "MM" method. Additionally, maintaining continuity conditions cannot be achieved solely with a transmitted field, leading to partial reflection of the incident field. Each mode undergoes scattering, resulting in a spectrum of transmitted and reflected modes. The initial step of the MM method involves expanding the unknown fields in individual duct regions using their respective modes. Given that the functional form of these modes is predetermined, the problem simplifies to determining modal amplitudes that correspond to field expansions in different waveguide regions. After establishing the modal representation, continuity conditions for the fields at junction interfaces are applied. By utilizing standard or generalized orthogonality relations of the modes, this process eventually results in an infinite system of linear simultaneous equations for the unknown modal amplitude. Eleftheriade et al. [65] work on mode matching technique for waveguide step discontinuities, ensuring

theoretical consistency and numerical accuracy. The study rigorously justifies the selection of testing modes and establishes the equivalence of two mode matching formulations. Additionally, it highlights the importance of mode selection in satisfying field boundary conditions and ensuring convergence.

2.8 Basic Definition

2.8.1 Waveguide

A waveguide is a structure designed to efficiently direct waves, such as electromagnetic or sound waves, while minimizing energy loss by confining their propagation to one or two dimensions. Its geometry is intricately tied to its function. In acoustics a waveguide operates similarly to a transmission line, facilitating the propagation of sound waves.

2.8.2 Amplitude

The amplitude of vibration represents the maximum distance a vibrating body moves from its equilibrium position.

2.8.3 Time period

The period of oscillation refers to the time required for a vibrating body to complete one full cycle of motion. Also known as the time period, it is represented by the symbol T.

$$T = \frac{2\pi}{\omega}. \tag{2.26}$$

Chapter 3

Wave Propagation in Permeable Membrane

In this chapter, we consider acoustic propagation and scattering through membrane interface. The governing ($BVPs$) include the Helmholtz equation, rigid conditions, membrane condition, and edge conditions. The eigen functions in respective duct regions are orthogonal in nature. The matching conditions together with well defined orthogonal characteristics lead to the solution of the problem. The procedure is discussed comprehensively in following sections. In Section 3.1, the scattering through the membrane interface in a continuous duct is given. Mode matching solution is discussed in Section 3.2. Sound power calculation is discussed in 3.3. The numerical results and discussion are given in last Section 3.4

3.1 Scattering through Membrane Interface in Continuous Duct

Consider an infinite cylindrical waveguide with radius $r = a$, having membrane at $z = 0$, as shown in Fig 3.1

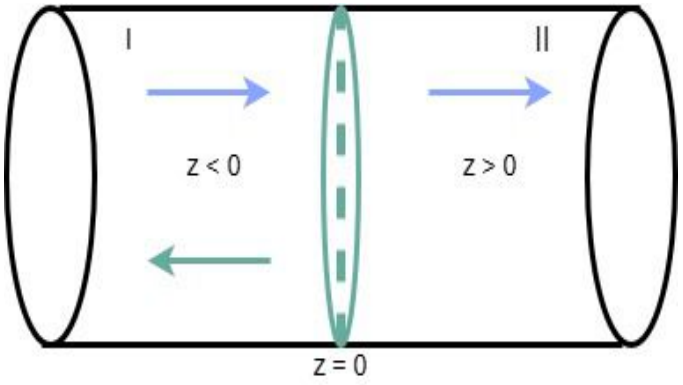

FIGURE 3.1: Flow Pattern Configuration.

The inside of waveguide is filled with compressible fluid of density ρ_0 and sound speed c. The dimensional wave equation for compressible fluid can be written as

$$\nabla^2 \tilde{P}(r,z,t) = \frac{1}{c^2}\frac{\partial^2 \tilde{P}}{\partial^2 t}. \tag{3.1}$$

The pressure $\tilde{P}$ with reference to duct regions I and II can be written as:

$$\tilde{P}(r,z,t) = \begin{cases} \tilde{P}_I(r,z,t), z < 0, 0 \leq r \leq a, \\ \tilde{P}_{II}(r,z,t), z > 0, 0 \leq r \leq a. \end{cases} \tag{3.2}$$

At $z = 0$, there exists a permeable membrane. The membrane displacement $\tilde{Y}(r,z,t)$ and $\tilde{U}(r,z,t)$ satisfy the equation

$$\nabla^2 \tilde{Y} + \frac{\rho_s}{T}\frac{\partial^2 \tilde{Y}}{\partial t^2} - \frac{R_f}{T}\frac{\partial(\tilde{Y}-\tilde{U})}{\partial t} = -\frac{(1-\Omega)}{T}(\tilde{P}_I - \tilde{P}_{II}), \tag{3.3}$$

and

$$\rho_0 \Omega h \frac{\partial^2 \tilde{U}}{\partial t^2} - R_f \frac{\partial(\tilde{Y}-\tilde{U})}{\partial t} = \Omega(\tilde{P}_I - \tilde{P}_{II}), \tag{3.4}$$

where

$$T = T_0(1 + j\eta), \Omega = N\pi a^2/A,$$

and

$$P_I - P_{II} = R_f v_f,$$

where T denote the tension in membrane having membrane density ρ_s, membrane viscosity η, thickness h, angular frequency ω and Ω is the dimenionless parameter.

R_f is the resistance to fluid flow through the membrane.

The continuities of velocity at the both side of a membrane at $z = 0$

$$-\frac{1}{i\omega\rho_0}\frac{\partial \tilde{P}_{II}}{\partial z} = (1-\Omega)\frac{\partial \tilde{Y}}{\partial t} + \Omega\frac{\partial \tilde{U}}{\partial t}, \tag{3.5}$$

$$-\frac{1}{i\omega\rho_0}\frac{\partial \tilde{P}_{I}}{\partial z} = (1-\Omega)\frac{\partial \tilde{Y}}{\partial t} + \Omega\frac{\partial \tilde{U}}{\partial t}. \tag{3.6}$$

On considering the harmonic time dependent $e^{-i\omega t}$, we write

$$\tilde{P}_I(r,z,t) = P_I(r,z)e^{-i\omega t}, \tag{3.7}$$

$$\tilde{P}_{II}(r,z,t) = P_{II}(r,z)e^{-i\omega t}, \tag{3.8}$$

$$\tilde{Y}(r,t) = Y(r)e^{-i\omega t}, \tag{3.9}$$

$$\tilde{U}(r,t) = U(r)e^{-i\omega t}. \tag{3.10}$$

With the aid of (3.7)-(3.10) the wave equation (3.11)

$$\left\{\nabla^2 + k^2\right\} P_j = 0, \tag{3.11}$$

where $j = I$ and $j = II$ represent the fluid pressure in region I and II, respectively such that

$$P(r,z) = \begin{cases} P_I(r,z), z < 0, 0 \le r \le a, \\ P_{II}(r,z), z > 0, 0 \le r \le a. \end{cases} \tag{3.12}$$

The membrane equation in harmonic time dependent form become

$$\nabla^2 Y + \frac{1}{T}\rho_s\omega^2 Y + \frac{i\omega R_f}{T}(Y-U) = -\frac{(1-\Omega)}{T}(P_I - P_{II}), \tag{3.13}$$

and

$$-\omega^2\rho_0\Omega h U + i\omega R_f(Y-U) = \Omega(P_I - P_{II}). \tag{3.14}$$

Accordingly, the continuities of velocity,

$$-\frac{1}{i\omega\rho_0}\frac{\partial P_I}{\partial z} = -(1-\Omega)i\omega Y - \Omega i\omega U, \tag{3.15}$$

and

$$-\frac{1}{i\omega\rho_0}\frac{\partial P_{II}}{\partial z} = -(1-\Omega)i\omega Y - \Omega i\omega U. \tag{3.16}$$

Further, the normal velocity at $z = 0$ are continuous, that gives

$$\frac{\partial P_I}{\partial z} = \frac{\partial P_{II}}{\partial z} \quad at \quad z = 0. \tag{3.17}$$

Let an incident wave strikes at membrane, a part is reflected in region I while rest is transmitted into the region II.

In order to analyze the reflection and transmission we solve the governing boundary value problem by using mode-matching technique. The solution is discussed in next section.

3.2 Mode Matching Solution

In this technique, first we apply the seperation of variable method and determine the eigenfunction expansion of fluid pressure in duct regions I and II. For region I, we assume

$$P_I(r,z) = R_1(r)Z_1(z). \tag{3.18}$$

On using (3.18) into (3.11), we get

$$\left(\frac{R_1''}{R_1} + \frac{1}{r}\frac{R_1'}{R_1} + \frac{Z_1''}{Z_1} + k^2\right) = 0, \tag{3.19}$$

$$\frac{R_1''}{R_1} + \frac{1}{r}\frac{R_1'}{R_1} + k^2 = -\frac{Z_1''}{Z_1} = \eta^2. \tag{3.20}$$

From (3.20), the solution of ordinary differential equation for $Z_1(z)$ is

$$Z_1(z) = c_1 e^{i\eta z} + c_2 e^{-i\eta z}, \tag{3.21}$$

where, for $R_1(r)$ the ordinary differential equation is

$$r^2R_1'' + rR_1' + r^2\tau^2 = 0 \text{ with } \tau = \sqrt{k^2 - \eta_n^2}, \tag{3.22}$$

which is a Bessel differential equation. The solution of equation (3.22) is

$$R_1(r) = c_3 J_0(\tau_r) + c_4 N_0(\tau_r), \tag{3.23}$$

where $J_0(\tau_r)$ and $N_0(\tau_r)$ are Bessel functions of first and second kind, respectively, and c_3 and c_4 are arbitrary constants. It is important to note that when $r \to 0$, the Bessel functions of second kind becomes undefined therefore, we choose $c_4 = 0$ for bounded solution and (3.23) becomes

$$R_1(r) = c_3 J_0(\tau_r). \tag{3.24}$$

Now to find c_3, we subsitute (3.24) into boundary condition. As the bounding surface is acoustically rigid, therefore, from (3.17) and (3.18), we get

$$R_1'(a) = 0. \tag{3.25}$$

By invoking (3.24), (3.25) for non-trivial solution leads to

$$J_0'(\tau a) = 0. \tag{3.26}$$

There are infinite many values of τ that satisfy (3.26), therefore $\tau \equiv \tau_n$ for n = 0, 1, 2 .... The resulting eigenfunction are

$$R_1 \equiv R_{1n}(r) = J_0(\tau_n r) \text{ for } n = 0, 1, 2 \ldots. \tag{3.27}$$

Hence, for $\tau = \tau_n$, the mode wave number

$$\eta \equiv \eta_n = \sqrt{k^2 - \tau_n^2}, \tag{3.28}$$

and (3.18) yields

$$P_1(r, z) = A_n R_{1n}(r) e^{i\eta_n z} + B_n R_{1n}(r) e^{-i\eta_n z}. \tag{3.29}$$

Note that first term of right hand side of (3.29) gives the expression for n^{th} propagating mode towards positive direction and second term on right hand sides stands for the n^{th} mode propagation in negative $z-$direction. The coefficients A_n and B_n are

amplitudes of n^{th} propagating modes. From superposition principle, the total field potential in region I can be given as

$$P_I(r,z) = \sum_{n=0}^{\infty} P_I(r,z). \tag{3.30}$$

Using (3.29) into (3.30)

$$P_I(r,z) = \sum_{n=0}^{\infty} \left\{ A_n e^{i\eta_n z} + B_n e^{i\eta_n z} \right\} R_{1n}(r). \tag{3.31}$$

Likewise for region II, we solve

$$\left\{ \frac{\partial^2}{\partial r^2} + \frac{1}{r}\frac{\partial}{\partial r} + \frac{\partial^2}{\partial z^2} + k^2 \right\} P_{II}(r,z) = 0, \tag{3.32}$$

subject to boundary condition

$$\frac{\partial P_{II}}{\partial r}(a,z) = 0, \tag{3.33}$$

and get:

$$P_{II}(r,z) = \sum_{n=0}^{\infty} \left\{ C_n e^{i\eta_n z} + D_n e^{-i\eta_n z} \right\} R_{2n}(r). \tag{3.34}$$

Note that (A_n, B_n, C_n, D_n) are unknowns. The corresponding eigenfunction in region I and II are identical, such that,

$$R_{1n}(r) = R_{2n}(r) = R_n(r).$$

We take the fundamental duct mode with unit amplitude from region I to positive z-direction, by setting $A_n = \delta_{n0}$ in (3.31). Furthermore we consider only transmission in region II by setting $D_n = 0$ in (3.34). Therefore, from (3.31) and (3.34) we get:

$$P_I(r,z) = e^{i\eta_0 z} + \sum_{n=0}^{\infty} B_n R_n(r) e^{-i\eta_n z}, \tag{3.35}$$

and

$$P_{II}(r,z) = \sum_{n=0}^{\infty} C_n R_n(r) e^{i\eta_n z}. \tag{3.36}$$

According to this condition, the eigenfunction $R_n(r) = J_0(\tau_n r), \quad n = 0, 1, 2, 3...$ subject to eigenvalues τ_n are orthogonal in nature and satisfy the appropriate orthogonality relation that can be derived from associated eigenvalue problem. For instance, for eigenvalues τ_n and eigenfunction $R_n(r) = J_0(\tau_n r)$, the associated eigenvalue problem is

$$R_n''(r) + \frac{1}{r}R_n'(r) + \tau_n^2 R_n(r) = 0, \tag{3.37}$$

$$R_n'(a) = 0. \tag{3.38}$$

To find orthogonality relation, on multiplying (3.38) with $aR_m(a)$, we get

$$R_n'(a)R_m(a) = 0. \tag{3.39}$$

By interchanging n by m we find

$$R_m'(a)R_n(a) = 0. \tag{3.40}$$

On subtracting (3.39) from (3.40), it is obviously obtain that

$$a\left[R_m'(a)R_n(a) - R_n'(a)R_m(a)\right] = 0, \tag{3.41}$$

or

$$\left[R_m'(a)R_n(a) - R_n'(a)R_m(a)\right]_{r=a}^{r=0} = 0. \tag{3.42}$$

By differentiating with respect to r, taking the integral, as well, (3.42) can be written to

$$\int_0^a \frac{d}{dr}\left[rR_m'(a)R_n(a) - R_n'(a)R_m(a)\right]dr = 0, \tag{3.43}$$

which on simplifications leads to

$$\int_0^a \left[rR_{1_n}(r)\left\{R_{1_m}''(r) + \frac{1}{r}R_{1_m}'(r)\right\} - rR_{1_m}(r)\left\{R_{1_n}''(r) + \frac{1}{r}R_{1_n}'(r)\right\}\right]dr = 0. \tag{3.44}$$

By using (3.37), (3.44) leads to

$$(\tau_n^2 - \tau_m^2) \int_0^a R_{1m}(r) R_{1n}(r) r dr = 0. \tag{3.45}$$

If $(\tau_n^2 - \tau_m^2) \neq 0$, then (3.45) leads to

$$\int_0^a R_{1m}(r) R_{1n}(r) r dr = 0. \tag{3.46}$$

If $(\tau_n^2 - \tau_m^2) = 0$, then integral takes the form

$$\int_0^a R_{1m}(r) R_{1n}(r) r dr = \int_0^a R_{1n}^2(r) = G_n, \tag{3.47}$$

where

$$G_n = \frac{a^2}{2} J_0^2(\tau_n a). \tag{3.48}$$

On combining (3.46) and (3.47), we get

$$\int_0^a R_{1m}(r) R_{1n}(r) r dr = \delta_{mn} G_n, \tag{3.49}$$

where δ_{mn} is Kronecker delta, that is

$$\delta_{mn} = \begin{cases} 0 \ m \neq n \\ 1 \ m = n. \end{cases} \tag{3.50}$$

Once the orthogonality relation is established, we can apply the interface conditions to determine $A_n, B_n, C_n \quad and \quad F_n$.

At the matching interface $z = 0$, an elastic membrane is present, whose displacement $Y(r)$ and $U(r)$ satisfies the equation.

3.2.1 Membrane Displacement Solution

The membrane displacements for solid component, $Y(r)$, and for fluid component, $U(r)$, can found through projection on orthogonal eigenfunction such that,

$$Y(r) = \sum_{n=0}^{\infty} A_n \xi_n(r), \tag{3.51}$$

and

$$U(r) = \sum_{n=0}^{\infty} F_n \xi_n(r), \tag{3.52}$$

where ξ_n satisfy the eigenvalue problem associate with membrane equation (3.13) and (3.14), that is

$$\frac{d^2\xi_n}{dr^2} + \frac{1}{r}\frac{d\xi_n}{dr} + \gamma_n^2 \xi = 0. \tag{3.53}$$

From (3.53) we get

$$\xi_n = J_0(\gamma_n r),$$

where γ_n, are found through the ring conditions at $r = a$ for fixed membrane

$$\xi_n(a) = 0.$$

1. Fixed edge

In case of fixed edges the displacements are zero, thus satisfy

$$Y_n(a) = 0, \tag{3.54}$$

since

$$\xi_n(a) = 0, \tag{3.55}$$

and γ_n are roots of

$$J_0(\gamma_n a) = 0.$$

It is also named as simply supported edge condition.

2. Free edge For free membrane the gradient is zero, that is

$$\frac{dY}{dr}(a) = 0. \tag{3.56}$$

Using (3.56) and we get

$$\xi_n'(a) = 0,$$

and γ_n are roots of

$$J_0'(\gamma_n a) = 0.$$

3. Spring like edge

The spring like condition satisfy the condition;

$$\frac{dY}{dr}(a) + \zeta Y(a) = 0, \tag{3.57}$$

where ζ, is coupling constant and γ_n, are roots of

$$J_0'(\gamma_n a) + \zeta J_0(\gamma_n a) = 0. \tag{3.58}$$

Note that ξ_n are orthogonal and satisfy the orthogonality relation;

$$\int_0^a \xi_n \xi_m r dr = \delta_{mn} E_n. \tag{3.59}$$

3.2.2 Interface Condition

We can apply interface conditions at $z = 0$ to find unknown amplitude, (A_n, B_n, C_n, D_n):

By substituting (3.35), (3.36), (3.52), and (3.53) into the membrane displacement (solid) (3.13), we found that

$$\begin{aligned} &\sum_{n=0}^{\infty} \left((\frac{d^2\xi_n}{dr^2} + \frac{1}{r}\frac{d\xi_n}{dr}) A_n + \frac{1}{T}\omega^2 \rho_s A_n + i\omega \frac{R_f}{T}(A_n - F_n) \right) \xi_n(r) \\ &= -\frac{(1-\Omega)}{T}(1 + \sum_{n=0}^{\infty}(B_n - C_n)) R_n(r). \end{aligned} \tag{3.60}$$

From (3.53) we have

$$\frac{d^2\xi_n}{dr^2} + \frac{1}{r}\frac{d\xi_n}{dr} = -\gamma_n^2 \xi. \tag{3.61}$$

By using, (3.61) into (3.60) we get

$$\begin{aligned}&\sum_{n=0}^{\infty}\Big(-\gamma_n^2 A_n+\frac{1}{T}\omega^2\rho_s A_n+i\omega\frac{R_f}{T}(A_n-F_n)\Big)\xi_n(r)\\&=-\frac{(1-\Omega)}{T}(1+\sum_{n=0}^{\infty}(B_n-C_n))R_n(r).\end{aligned}\tag{3.62}$$

On multiplying (3.62) by $r\xi_m(r)$ and integrating from 0 to a it is found that

$$\begin{aligned}&\sum_{n=0}^{\infty}\Big((-\gamma_n^2 A_n+\omega^2\frac{\rho_s}{T}A_n+i\omega\frac{R_f}{T}(A_n-F_n)\Big)\int_0^a\xi_n(r)\xi_m(r)rdr\\&=-\frac{(1-\Omega)}{T}(1+\sum_{n=0}^{\infty}(B_n-C_n))\int_0^a R_n(r)\xi_m(r)rdr.\end{aligned}\tag{3.63}$$

On using orthogonality relation, (3.63) gives

$$\begin{aligned}&\Big(-\gamma_m^2+\omega^2\frac{\rho_s}{T}+i\omega\frac{R_f}{T}\Big)A_m-i\omega\frac{R_f}{T}F_m\\&=-\frac{(1-\Omega)}{TE_m}\big(L_{0n}+\sum_{n=0}^{\infty}(B_n-C_n)L_{nm}\big),\end{aligned}\tag{3.64}$$

where

$$L_{0n}=\int_0^a\xi_m(r)rdr,$$

$$L_{nm}=\int_0^a R_n(r)\xi_m(r)rdr.$$

By substituting (3.35), (3.36), (3.52), and (3.53) into the membrane displacement (fluid) (3.14), and we get:

$$\sum_{n=0}^{\infty}\Big(-\omega^2\rho_0\Omega hF_n+i\omega R_f(A_n-F_n)\Big)\xi_n(r)=\Omega\big(1+\sum_{n=0}^{\infty}(B_n-C_n)\big)R_n(r).\tag{3.65}$$

Multiplying (3.65) with $r\xi_m(r)$ and integrating $0 \leq r \leq a$ we get

$$\begin{aligned}&\sum_{n=0}^{\infty}\Big(-\omega^2\rho_0\Omega h F_n + i\omega R_f(A_n - F_n)\Big)\int_0^a \xi_n(r)\xi_m(r)rdr\\&= \Omega\big(1+\sum_{n=0}^{\infty}(B_n - C_n)\big)\int_0^a R_n(r)\xi_m(r)rdr.\end{aligned} \tag{3.66}$$

On using orthogonality relation, (3.66) gives

$$-\omega^2\rho_0\Omega h F_m + i\omega R_f(A_m - F_m) = \frac{\Omega}{E_m}\left(L_{0n} + \sum_{n=0}^{\infty}(B_n - C_n)L_{nm}\right), \tag{3.67}$$

where

$$L_{0n} = \int_0^a \xi_m(r)rdr,$$

$$L_{nm} = \int_0^a R_n(r)\xi_m(r)rdr.$$

By simplification (3.35), (3.36), (3.52), and (3.52) into (3.15) and after some arrangement we found

$$-\frac{1}{\omega\rho_0}\left(\eta_0 - \sum_{n=0}^{\infty}\eta_n B_n R_n(r)\right) = i\omega\sum_{n=0}^{\infty}\Big((1-\Omega)A_n - (\Omega)B_n\Big)\xi_n(r). \tag{3.68}$$

Multiplying (3.68) with $rR_m(r)$ and integrating $0 \leq r \leq a$ and we get

$$\begin{aligned}&-\frac{1}{\omega\rho_0}\left(\eta_0\int_0^a R_m(r)rdr - \sum_{n=0}^{\infty}B_n\eta_n\int_0^a R_n(r)R_m(r)rdr\right)\\&= i\omega\sum_{n=0}^{\infty}\Big((1-\Omega)A_n - \Omega B_n\Big)\int_0^a \xi_n(r)R_m(r)rdr.\end{aligned} \tag{3.69}$$

On using orthogonality relation, (3.69) gives

$$-\frac{1}{\omega\rho_0}\Big(\eta_0\delta_{m0} - B_m G_m\Big) = i\omega\sum_{n=0}^{\infty}\Big((1-\Omega)A_n - \Omega B_n\Big)L_{nm}, \tag{3.70}$$

where

$$L_{nm} = \int_0^a \xi_n(r)R_m(r)rdr. \tag{3.71}$$

By simplification (3.35), (3.36), (3.52), and (3.53) into the continuity of velocity in membrane (3.16), we found

$$-\frac{1}{\omega\rho_0}\sum_{n=0}^{\infty}C_n\eta_nR_n(r)=i\omega\sum_{n=0}^{\infty}\Big((1-\Omega)A_n-(\Omega)B_n\Big)\xi_n(r). \tag{3.72}$$

Multiplying (3.72) with $rR_m(r)$ and integrating $0\leq r\leq a$ we get

$$\begin{aligned}&-\frac{1}{\omega\rho_0}\sum_{n=0}^{\infty}\eta_nC_n\int_0^a R_n(r)R_m(r)rdr\\&=i\omega\sum_{n=0}^{\infty}\Big((1-\Omega)A_n-(\Omega)B_n\Big)\int_0^a\xi_n(r)R_m(r)rdr.\end{aligned} \tag{3.73}$$

By using orthogonality relation on (3.73) and found

$$-\frac{1}{\omega\rho_0}C_m\eta_m=\frac{i\omega}{G_m}\sum_{n=0}^{\infty}\Big((1-\Omega)A_n-\Omega B_n\Big)L_{nm}. \tag{3.74}$$

By invoking (3.35), (3.36), (3.52), and (3.53) into the normal velocity (3.17), the resulting equation is

$$\frac{\partial}{\partial z}\Big(e^{i\eta_0 z}+\sum_{n=0}^{\infty}B_nR_n(r)e^{-i\eta_n z}\Big)=\frac{\partial}{\partial z}\Big(\sum_{n=0}^{\infty}C_nR_n(r)e^{i\eta_n z}\Big). \tag{3.75}$$

From (3.75)

$$\eta_0-\sum_{n=0}^{\infty}B_n\eta_nR_n(r)=\sum_{n=0}^{\infty}C_n\eta_nR_n(r). \tag{3.76}$$

Multiplying (3.76) with $rR_m(r)$ and integrating $0\leq r\leq a$

$$\eta_0\int_0^a R_m(r)dr-\sum_{n=0}^{\infty}B_n\eta_n\int_0^a R_mR_n(r)rdr=\sum_{n=0}^{\infty}C_n\eta_n\int_0^a R_mR_n(r)rdr. \tag{3.77}$$

By using orthogonality relation on (3.77)

$$\eta_0G_m\delta_{m0}-B_m\eta_mG_m=C_m\eta_mG_m, \tag{3.78}$$

or

$$\eta_0 \delta_{m0} = B_m \eta_m + C_m \eta_m. \tag{3.79}$$

3.3 Sound Power Calculation

To analyze problem physically, the sound power expressions are calculated by using acoustical solution with power calculated using membrane based solution.

$$W = 2\pi\omega\rho \,\mathrm{Re}\left[\int_\Omega i\bar{\phi}\left(\frac{\partial\bar{\phi}}{\partial\bar{z}}\right)^* r d\bar{r}\right], \tag{3.80}$$

where ω is the region. By non-dimensionalizing under the transformation given in (3.1), we get

$$W = \frac{2\pi\omega^3\rho}{k^5} \,\mathrm{Re}\left[\int_\Omega i\bar{\phi}\left(\frac{\partial\phi}{\partial z}\right)^* r dr\right]. \tag{3.81}$$

By using $\omega = ck$ in equation (3.81) we get

$$W = \frac{2\pi c^3\rho}{k^2} \,\mathrm{Re}\left[\int_\Omega i\bar{\phi}\left(\frac{\partial\phi}{\partial z}\right)^* r dr\right]. \tag{3.82}$$

That gives non-dimensional energy flux

$$W = \mathrm{Re}\left[\int_\Omega i\bar{\phi}\left(\frac{\partial\phi}{\partial z}\right)^* r dr\right], \tag{3.83}$$

where $W = \dfrac{k^2\bar{W}}{2\pi c^3\rho}$. Now by using incident field as $P_{inc} = e^{iz}$ in (3.83), leads to incident power

$$W_{d,a} = \mathrm{Re}\left\{\int_0^a e^{iz}(-ie^{-iz}) r dr\right\}, \tag{3.84}$$

or

$$W_{d,a} = \frac{a^2}{2}. \tag{3.85}$$

Similarly we have calculate the W_I as transmitted, and W_{II} as reflected.

3.3.1 Sound Field Based Solution

The sound power entering region I (W_I) is calculated by integrating the product of the incident sound pressure (P_I) and the complex conjugate of the particle velocity (u_I^*) over the membrane's surface area.

$$W_I = \frac{1}{2} Re \int_0^a P_I(u_I^*)(2\pi r)dr, \tag{3.86}$$

where superscript asterisk (*) denotes the complex conjugate. From the definition of energy flux/power,the incident power is found to be W_{inc}. Likewise, the power/energy flux components in duct region $R_j, j = 1, 2$ are:

$$W_I = \frac{1}{2} Re \sum_{m,n=0}^{\infty} B_n B_m^* e^{-i(\eta_n - \eta_m^*)z} \eta_m^* (2\pi) \int_0^a R_{1n}(r) R_{1m}(r) r dr. \tag{3.87}$$

Apply orthogonality relation, (3.87) gives;

$$W_I = Re \left[\sum_{n=0}^{\infty} |B_n|^2 \eta_m^* e^{-i(\eta_n - \eta_m^*)z} G_m \right], \tag{3.88}$$

as $\eta_n = \sqrt{k^2 - \tau_n^2}$ is either real or pure imaginary. Therefore, (3.88) yields

$$W_I = Re \left[\sum_{n=0}^{\infty} |B_n|^2 \eta_n G_m \right]. \tag{3.89}$$

Similarly we have, the sound power transmitted into region II (W_{II}) is determined by integrating the transmitted sound pressure (P_{II}) and the complex conjugate of the particle velocity (u_{II}^*)

$$W_{II} = \frac{1}{2} Re \sum_{m,n=0}^{\infty} C_n C_m^* e^{-i(\eta_n - \eta_m^*)z} \eta_m^* (2\pi) \int_0^a R_{1n}(r) R_{1m}(r) r dr. \tag{3.90}$$

Note that, as τ_n, $n = 0, 1, 2$ are real which implies $R_{1m} = J_0(\tau_m r)$, also $R_{1m}^* = R_{1m}$ and thus, (3.90) gives

$$W_{II} = \frac{1}{2} Re \sum_{m,n=0}^{\infty} C_n C_m^* e^{-i(\eta_n - \eta_m^*)z} \eta_m^* (2\pi) \int_0^a R_{1n}(r) R_{1m}(r) r dr. \tag{3.91}$$

On using orthogonality relation, (3.91) gives

$$W_{II} = Re\left[\sum_{n=0}^{\infty} |C_n|^2 \eta_n G_m\right]. \tag{3.92}$$

Power dissipated

$$W_{d,a} = W_I - W_{II}. \tag{3.93}$$

Using (3.89) and (3.92) into (3.93) we get

$$W_{d,a} = \left[\sum_{n=0}^{\infty} |B_n|^2 \eta_n G_m\right] - \left[\sum_{n=0}^{\infty} |C_n|^2 \eta_n G_m\right]. \tag{3.94}$$

3.3.2 Membrane Based Solution

Solid Component Dissipation: This accounts for the power dissipated due to the membrane's structural vibration.

$$W_{d,m,solid} = \frac{1}{2} Re\left\{ \int_0^a T\left[\nabla^2 y + k_f^2 y - \frac{\rho_0 \Omega h}{T} \frac{\partial (y-u)}{\partial t}\right] \frac{\partial y^*}{\partial t} (2\pi r) dr \right\}. \tag{3.95}$$

Fluid Component Dissipation: This represents the power loss due to the oscillatory flow of fluid through the membrane's pores.

$$W_{d,m,fluid} = \frac{1}{2} Re\left\{ \int_0^a \left[\rho_0 \Omega h \frac{\partial^2 u}{\partial t^2} - R_f \frac{\partial (y-u)}{\partial t}\right] u^* (2\pi r) dr \right\}. \tag{3.96}$$

Total Dissipated Power (Membrane): The total power dissipated by the membrane is the sum of the solid and fluid components:

$$W_{d,m} = W_{d,m,solid} + W_{d,m,fluid}. \tag{3.97}$$

3.4 Numerical Results and Discussions

Here the problem is solved numerically after making truncation of equations upto some N terms. The systems are solved using MATHEMATICA solver "NSolve". The are various parameters in the equations that are given numerical values. These

numerical values are given in reference [66]. The particular values are taken as follows: $a = 0.05\,\text{m}$, $\rho_s = 0.174\,\text{kg/m}^2$, $T_0 = 85\,\text{N/m}$, $\eta = 0.005$, $\Omega = 0.0018$, $R_f = 0.15\,\text{Rayls}$, $h = 0.2\,\text{mm}$. The number of terms are taken to 10 terms. In Fig. 3.2, the real parts of normal velocities are shown against radius r at frequency $f = 100$ Hz.

Both velocity components coincide which validates the truncated solution at the given frequency. In Fig. 3.3, the real parts of normal velocities are shown against radius r at frequency $f = 1000$ Hz. More modes are excited by increasing frequency while velocity components coincide which validates the truncated solution at $f = 1000$ Hz.

In Fig. 3.4, the real parts of normal velocities are shown against radius r at frequency $f = 2500$ Hz. On increasing frequency the number of propagating modes are increased. Both velocity components coincide which validates the truncated solution at the given frequency. "Note that here $\phi_1 = P_I$ and $\phi_2 = P_{II}$."

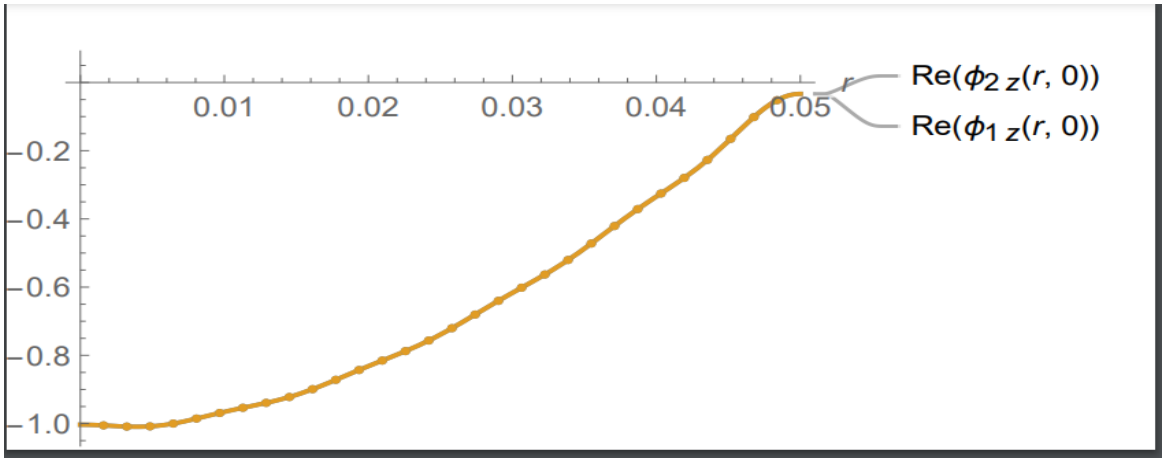

FIGURE 3.2: Real parts of the velocities against r at $f = 100$ Hz

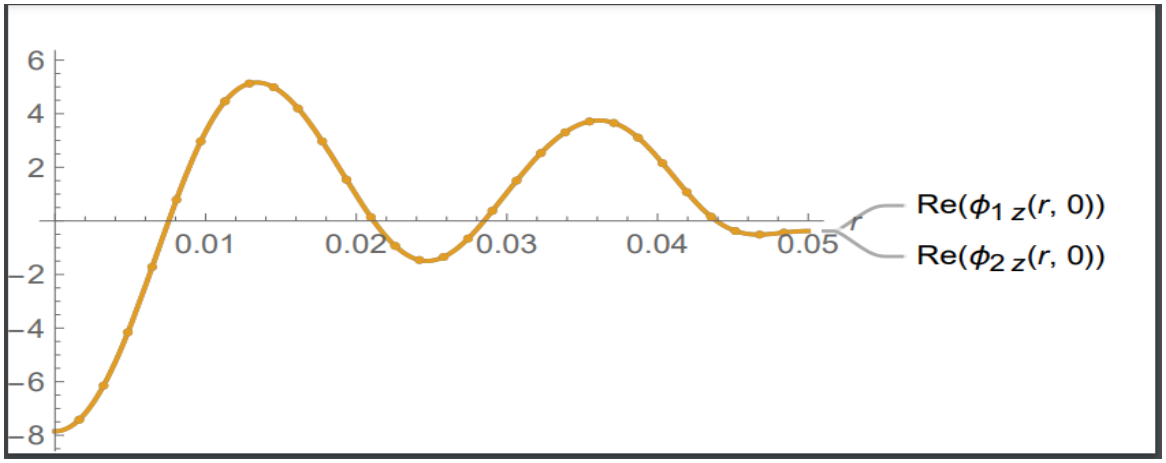

FIGURE 3.3: Real parts of the velocities against r at $f = 1000$ Hz

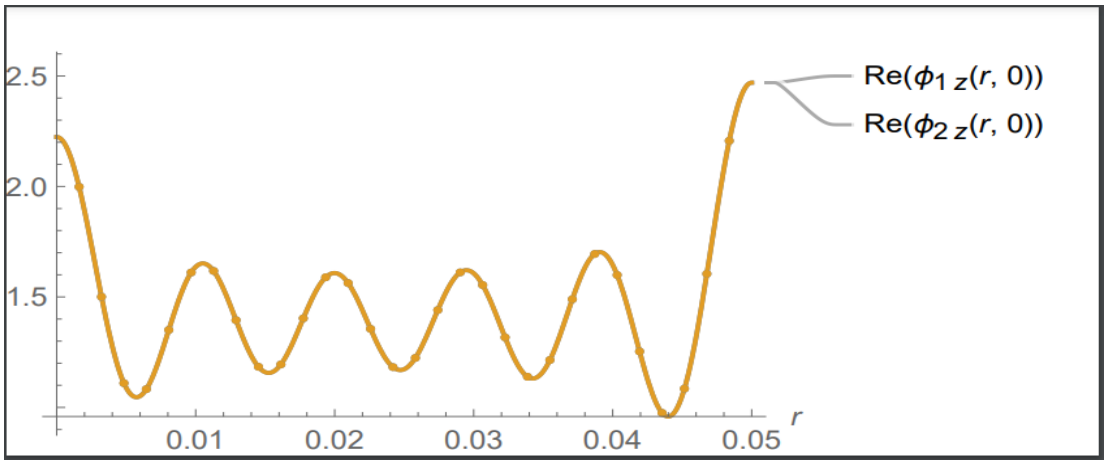

FIGURE 3.4: Real parts of the velocities against r at $f = 2500$ Hz

The imaginary parts of the normal velocities are examined at various frequencies to further validate the truncated solution. Figs. 3.5 - 3.7 at frequencies $f = 100$, 1000, and 2500 Hz, respectively. At each frequency, the coincidence of velocity components is observed, indicating that the truncated solution accurately captures the dynamics of the system.

Moreover, the results reveal that increasing the frequency excites additional modes, as evident from the growing number of propagating modes in the velocity profiles (Figs. 3.6 and 3.7). This trend is consistently observed across the three frequencies, demonstrating the robustness of the solution.

The presence of additional modes at higher frequencies highlights the importance of considering the effects of frequency on the dynamics of the system.

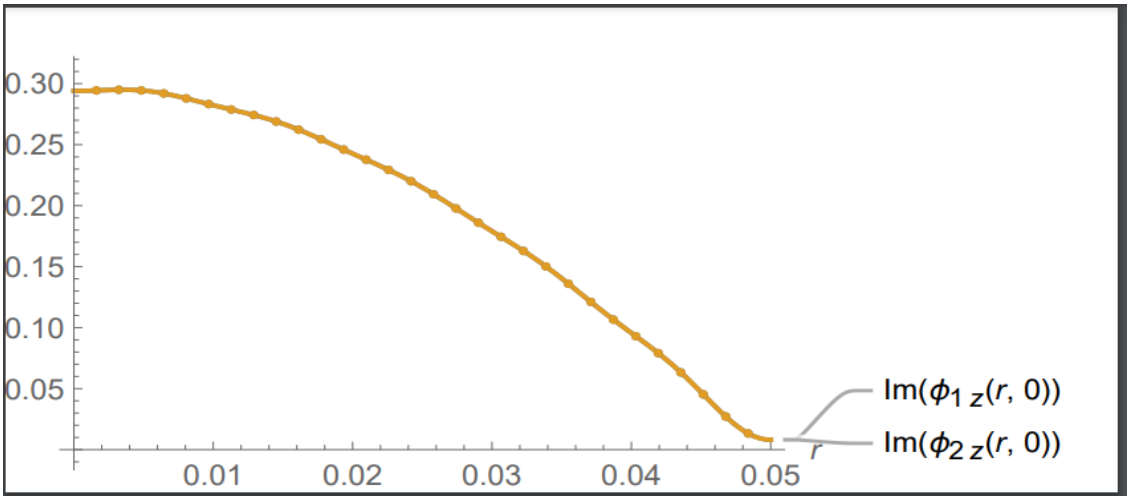

FIGURE 3.5: Imaginary parts of the velocities against r at $f = 100$ Hz

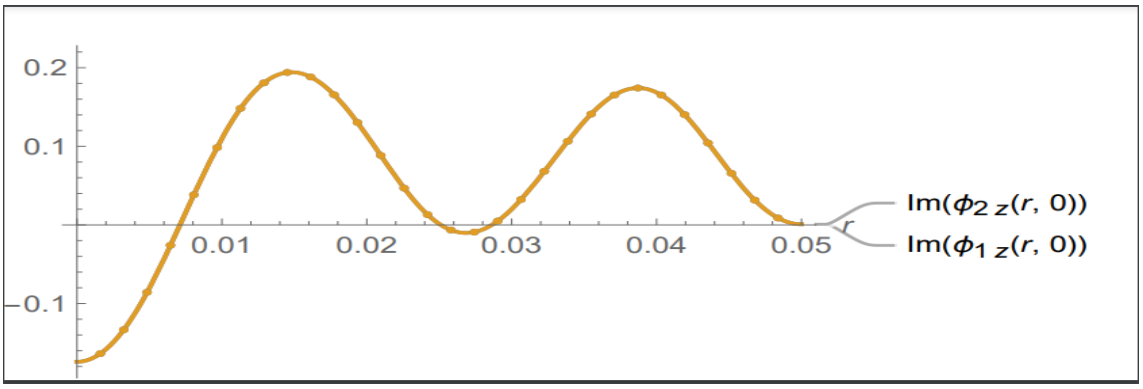

FIGURE 3.6: Imaginary parts of the velocities against r at $f = 1000$ Hz

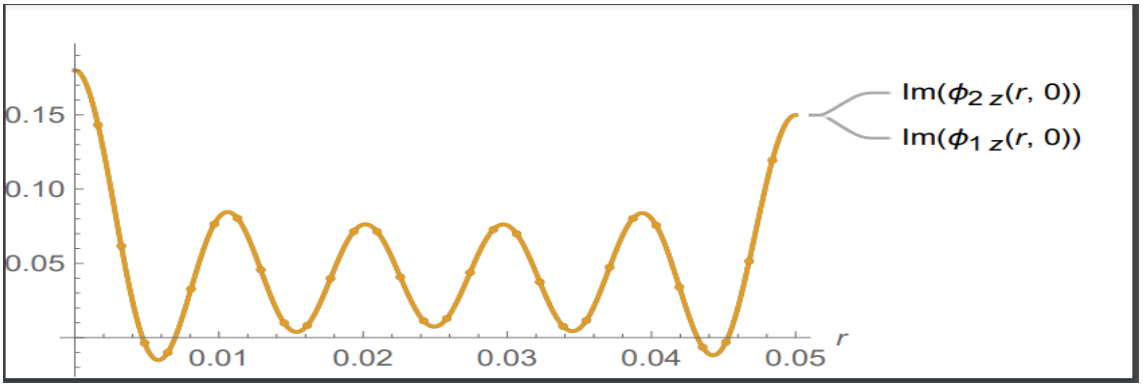

FIGURE 3.7: Imaginary parts of the velocities against r at $f = 2500$ Hz

The numerical results presented in this study demonstrate the effectiveness of the proposed approach in capturing the complex dynamics of the fluid-structure interaction system. The coincidence of velocity components at each frequency validates the truncated solution, indicating that the proposed approach accurately captures the dynamics of the system. Furthermore, the results reveal that increasing the frequency excites additional modes. This trend is consistently observed across the three frequencies, demonstrating the robustness of the solution. The presence of additional modes at higher frequencies highlights the importance of considering the effects of frequency on the dynamics of the system. The findings of this study provide valuable insights into the complex dynamics of fluid-structure interaction systems and demonstrate the effectiveness of the proposed approach in capturing these dynamics.

Chapter 4

Mode Filtering using Permeable Membrane Cavity

In this chapter, we examine the propagation and scattering of acoustic waves with membranes at interfaces that include rigid boundaries. The first problem addresses the acoustic membrane in a rigid cavity, while the second problem involves the response of permeable membrane backed by soft cavity. Section 4.1 presents the mathematical modeling of problem formulation. In Section 4.2, the modeling of the response of a permeable membrane backed by a rigid cavity. Section 4.3, modeling of the response of a permeable membrane backed by a soft cavity is explored.

4.1 Problem Formulation

The problem described in this section involves analyzing a membrane at interfaces. It is important to note that all the boundaries of the waveguide are rigid and the interior of the waveguide is filled with compressible fluid. The waveguide is divided into three regions:

In region I $(0 < r < a, z < -L)$, the pressure is indicated by $P_I(r, z)$ in region II $(0 < r < a, -L < z < L)$, the pressure is represented by $P_{II}(r, z)$ and in region III $(0 < r < a, L = 0)$, the pressure is given by $P_{III}(r, z)$.

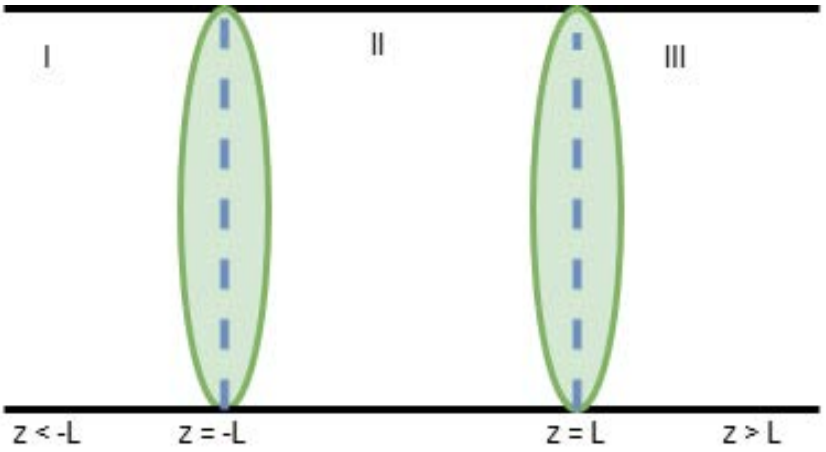

FIGURE 4.1: The physical Configuration waveguide.

The governing boundary value problem consists of the Helmholtz equation, along with rigid boundary conditions and membrane conditions such as:

$$\left\{\frac{\partial^2}{\partial r^2}+\frac{1}{r}\frac{\partial}{\partial r}+\frac{\partial^2}{\partial z^2}+k^2\right\}P_j(r,z)= \quad j=1,2,3 \tag{4.1}$$

$$\frac{\partial P_j}{\partial z}=0, \quad r=a. \tag{4.2}$$

By solving (4.1) subject to the condition in (4.2) using the separation of variables technique, we can drive the expansion of the eigenfunction for the fundamental mode. This is given by:

$$P_I(r,z)=e^{i\eta_0(z+L)}+\sum_{n=0}^{\infty}B_n e^{-i\eta_n(z+L)}, \tag{4.3}$$

where $\eta_n=\sqrt{k^2-\tau_n^2}$ is the wave number for the n^{th} mode propagating in region I, with amplitude B_n. The eigenvalues τ_n are the roots of:

$$J_0'(\tau_n a)=0.$$

For region II, the non-dimensional Helmholtz equation and rigid boundary condition are

$$\left\{\frac{\partial^2}{\partial r^2}+\frac{1}{r}\frac{\partial}{\partial r}+\frac{\partial^2}{\partial z^2}+k^2\right\}P_{II}(r,z)=0, \tag{4.4}$$

$$\frac{\partial P_{II}}{\partial z}=0, \quad r=a. \tag{4.5}$$

By solving (4.4) subject to (4.5) with separation of variable technique for fundamental mode incident we can get eigenfunction expansion as

$$P_{II}(r,z) = \sum_{n=0}^{\infty} C_n R_n(r) e^{i\eta_n z} + \sum_{n=0}^{\infty} D_n R_n(r) e^{-i\eta_n z}, \tag{4.6}$$

where, C_n and D_n are amplitudes of reflected and transmitted modes and are unknowns.

The corresponding eigenfunction $R_n(r)$ satisfy orthogonality relation. From equation (4.1) and (4.2), the eigenfunction expansions of the field potential in region region III are as follows

and

$$P_{III}(r,z) = \sum_{n=0}^{\infty} H_n e^{i\eta_n(z-L)} R_{3n}(r), \tag{4.7}$$

respectively.

The coefficient H_n represents the amplitude of the n^{th} mode propagating in region III. The corresponding eigenfunction $R_{3n}(r) = J_0(\tau_n r)$ for n = 0,1,2...

The eigenfunction in region I, II and III are identical, such that:

$$R_{1n}(r) = R_{2n}(r) = R_{3n}(r) = R_n(r).$$

The corresponding eigenfunctions $R_n(r)$ satisfy orthogonality relation

$$\int_0^a R_m(r) R_n(r) r dr = \delta_{mn} G_n. \tag{4.8}$$

Note that $(A_n, B_n, C_n, D_n, H_n)$ are unknown and will be determined using the mode-matching technique. That will be found through mode-matching technique.

Before applying this procedure, we divide the given membrane into two sub-cavity.

- Response of a permeable membrane backed by a rigid cavity
- Response of a permeable membrane backed by a soft cavity

4.2 Response of a Permeable Membrane Backed by a Rigid Cavity

In this setting we assume rigid disc at $z = -L$. And the soft wall at $z = 0$. The physical configuration of the soft cavity is as shown in Fig 4.2

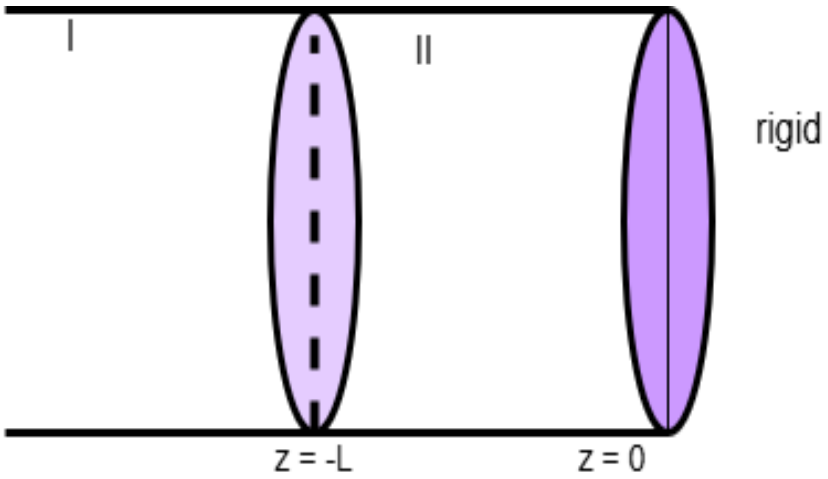

FIGURE 4.2: The physical Configuration of rigid cavity.

we consider the Helmholtz equation, rigid condition and membrane condition for region II are as follows:

$$\left\{\frac{\partial^2}{\partial r^2}+\frac{1}{r}\frac{\partial}{\partial r}+\frac{\partial^2}{\partial z^2}+k^2\right\}P_{II}(r,z)=0, \tag{4.9}$$

$$\frac{\partial P_{II}}{\partial z}(r,0)=0. \tag{4.10}$$

By using (4.10) into (4.9), we get

$$\sum_{n=0}^{\infty} C_n\eta_n R_{2n}(r)-\sum_{n=0}^{\infty} D_n\eta_n R_{2n}(r). \tag{4.11}$$

From (4.11) we get

$$C_n = D_n. \tag{4.12}$$

On using (4.12) into (4.6), we modify the pressure $P_{II}(r,z)$ as:

$$P_{II}(r,z) = 2\sum_{n=0}^{\infty} C_n \cos(s_n z) R_{2n}(r). \tag{4.13}$$

For rigid cavity case we use superscript "s" on variables, such that then the acoustic potentials in rigid cavity take formulation as

$$P_I^s(r,z) = e^{i\eta_0(z+L)} + \sum_{n=0}^{\infty} B_n^s e^{-i\eta_n(z+L)} R_{1n}, \tag{4.14}$$

and

$$P_{II}^s(r,z) = 2\sum_{n=0}^{\infty} C_n^s \cos(s_n z) R_{2n}(r). \tag{4.15}$$

Likewise the membrane displacement is

$$Y^s(r) = \sum_{n=0}^{\infty} A_n^s \xi_n(r), \tag{4.16}$$

and

$$U^s(r) = \sum_{n=0}^{\infty} F_n^s \xi_n(r). \tag{4.17}$$

Note that the quantities A_n^s, B_n^s, C_n^s and F_n^s are amplitudes of rigid modes and will be found through the interface conditions.

As we have assumed the membrane interfaces at $z = -L$ with rigid cavity configuration the membrane displacement equation and is:

$$\nabla^2 Y + \frac{1}{T}\rho_s \omega^2 Y + \frac{i\omega R_f}{T}(Y - U) = -\frac{(1-\Omega)}{T}(P_I - P_{II}), \tag{4.18}$$

and

$$-\omega^2 \rho_0 \Omega h U + i\omega R_f (Y - U) = \Omega(P_I - P_{II}). \tag{4.19}$$

Accordingly, the continuities of velocity

$$-\frac{1}{i\omega\rho_0}\frac{\partial}{\partial z}P_I = -(1-\Omega)i\omega Y - \Omega i\omega U, \tag{4.20}$$

$$-\frac{1}{i\omega\rho_0}\frac{\partial}{\partial z}P_{II} = -(1-\Omega)i\omega Y - \Omega i\omega U. \tag{4.21}$$

Further, the normal velocity

$$\frac{\partial P_I}{\partial z} = \frac{\partial P_{II}}{\partial z} \quad at \quad z = 0. \tag{4.22}$$

The membrane equation derived by substituting (4.14), (4.15), (4.16), and (4.17) into the membrane displacement (solid) (4.18). Resulting is the following:

$$\begin{aligned}&\sum_{n=0}^{\infty}\left(-\gamma_n^2 A_n^s + \omega^2\frac{\rho_s}{T}A_n^s + i\omega\frac{R_f}{T}(A_n^s - F_n^s)\right)\xi_n(r)\\ &= -\frac{(1-\Omega)}{T}\left(1 + \sum_{n=0}^{\infty}B_n^s R_n(r) - 2\sum_{n=0}^{\infty}C_n^s\cos(s_n L)R_n(r)\right).\end{aligned} \tag{4.23}$$

On multiplying (4.23) by $r\xi_m(r)$ and integrating from 0 to a, we obtain:

$$\begin{aligned}&\sum_{n=0}^{\infty}\left((-\gamma_n^2 A_n^s + \omega^2\frac{\rho_s}{T}A_n^s + i\omega\frac{R_f}{T}(A_n^s - F_n^s)\right)\int_0^a \xi_n(r)\xi_m(r)rdr\\ &= -\frac{(1-\Omega)}{T}\left(1 + \sum_{n=0}^{\infty}B_n^s - 2\sum_{n=0}^{\infty}C_n^s\cos(s_n L)\right)\int_0^a R_n(r)\xi_m(r)rdr.\end{aligned} \tag{4.24}$$

Applying the orthogonality relation on (4.24), we simplify the equation (4.24) as

$$\begin{aligned}&\left(-\gamma_n^2 A_m^s + \omega^2\frac{\rho_s}{T}A_m^s + i\omega\frac{R_f}{T}(A_m^s - F_m^s)\right)\\ &= -\frac{(1-\Omega)}{TE_m}\left(L_{n0} + \sum_{n=0}^{\infty}B_n^s - 2\sum_{n=0}^{\infty}C_n^s\cos(s_n L)L_{nm}\right),\end{aligned} \tag{4.25}$$

where

$$L_{0n} = \int_0^a \xi_m(r)rdr,$$

$$L_{nm} = \int_0^a R_n(r)\xi_m(r)rdr.$$

By substituting (4.14), (4.15), (4.16) and (4.17), into the membrane displacement

(fluid) (4.19) and we get

$$\begin{aligned}\sum_{n=0}^{\infty}\Big(-\omega^2\rho_0\Omega h F_n^s + i\omega R_f(A_n^s - F_n^s)\Big)\xi_n(r)\\ = \Omega\big(1+\sum_{n=0}^{\infty}B_n^s - 2\sum_{n=0}^{\infty}C_n^s\cos(s_nL)\big)R_n(r).\end{aligned} \tag{4.26}$$

Multiplying (4.26) with $r\xi_m(r)$ and integrating $0 \le r \le a$ we get

$$\begin{aligned}\sum_{n=0}^{\infty}\Big(-\omega^2\rho_0\Omega h F_n^s + i\omega R_f(A_n^s - F_n^s)\Big)\int_0^a \xi_n(r)\xi_m(r)rdr\\ = \Omega\big(1+\sum_{n=0}^{\infty}B_n^s - 2\sum_{n=0}^{\infty}C_n^s\cos(s_nL)\big)\int_0^a R_n(r)\xi_m(r)rdr.\end{aligned} \tag{4.27}$$

On using orthogonality relation, (4.27) gives

$$\Big(-\omega^2\rho_0\Omega h F_m^s + i\omega R_f(A_m^s - F_m)^s\Big) = \frac{\Omega}{E_m}\Big(L_{n0} + \sum_{n=0}^{\infty}B_n^s - 2\sum_{n=0}^{\infty}C_n^s\cos(s_nL)L_{nm}\Big), \tag{4.28}$$

where

$$L_{n0} = \int_0^a \xi_m(r)rdr,$$

and

$$L_{nm} = \int_0^a R_n(r)\xi_m(r)rdr.$$

By simplification (4.14), (4.15), (4.16), and (4.17) into (4.20) and after some arrangement we found

$$\frac{i}{\omega^2\rho_0}\Big(\eta_0 - \sum_{n=0}^{\infty}B_n^s\eta_n R_n(r)\Big) = \sum_{n=0}^{\infty}\Big((1-\Omega)A_n^s - (\Omega)B_n^s\Big)\xi_n(r). \tag{4.29}$$

Multiplying (4.29) with $rR_m(r)$ and integrating $0 \le r \le a$ and we get

$$\begin{aligned}\frac{i}{\omega^2\rho_0}\Big(\eta_0\int_0^a R_m(r)rdr - \sum_{n=0}^{\infty}B_n^s\eta_n\int_0^a R_n(r)R_m(r)rdr\Big)\\ = \Big((1-\Omega)A_n^s - \Omega B_n^s\Big)\int_0^a \xi_n(r)R_m(r)rdr.\end{aligned} \tag{4.30}$$

On using orthogonality relation, (4.30) gives

$$\frac{i}{\omega^2\rho_0}\left(\eta_0\delta_{n0} - B_m^s\eta_m G_m\right) = \sum_{n=0}^{\infty}\left((1-\Omega)A_n^s - \Omega B_n^s\right)L_{nm}. \tag{4.31}$$

By simplification (4.14), (4.15), (4.16), and (4.17) into the continuity of velocity in membrane (4.21) we found

$$\frac{1}{\omega^2\rho_0}2\sum_{n=0}^{\infty}C_n^s\sin(s_nL)s_nR_n(r) = \sum_{n=0}^{\infty}\left((1-\Omega)A_n - (\Omega)B_n^s\right)\xi_n(r). \tag{4.32}$$

Multiplying (4.32) with $rR_m(r)$ and integrating $0 \le r \le a$ we get

$$\begin{aligned}&\frac{1}{\omega^2\rho_0}2\sum_{n=0}^{\infty}s_nC_n^s\sin(s_nL)\int_0^a R_n(r)R_m(r)rdr\\ &=\sum_{n=0}^{\infty}\left((1-\Omega)A_n^s - (\Omega)B_n^s\right)\int_0^a \xi_n(r)R_m(r)rdr.\end{aligned} \tag{4.33}$$

By using orthogonality relation on (4.33) and found

$$\frac{2s_m}{\omega^2\rho_0}C_m^s\sin(s_mL) = \frac{i\omega}{G_m}\left((1-\Omega)A_n^s - \Omega B_n^s\right)L_{nm}, \tag{4.34}$$

where

$$\delta_{n0} = \int_0^a R_m(r)rdr.$$

By invoking (4.14), (4.15), (4.16), and (4.17) into the normal velocity (4.22) the resulting equation is

$$i\left(\eta_0 - \sum_{n=0}^{\infty}B_n^s\eta_nR_n(r)\right) = 2\sum_{n=0}^{\infty}s_nC_n^s\sin(s_nL)R_n(r). \tag{4.35}$$

Multiplying equation (4.35) by $rR_m(r)$, integrating over $0 \le r \le a$, we obtain;

$$\begin{aligned}&i\left(\eta_0\int_0^a R_m(r)rdr - \sum_{n=0}^{\infty}B_n^s\eta_n\int_0^a R_n(r)R_m(r)rdr\right)\\ &=2\sum_{n=0}^{\infty}s_nC_n^s\sin(s_nL)\int_0^a R_n(r)R_m(r)rdr.\end{aligned} \tag{4.36}$$

And applying the orthogonality relation on (4.36), we get;

$$i(G_m\delta_{n0} - B_m^s\eta_mG_m) = 2s_mC_m^s\sin(s_mL)G_m. \tag{4.37}$$

4.3 Response of a Permeable Membrane Backed by Soft Cavity

The response of permeable membrane backed by soft cavity can be considered by assuming the rigid disc at $z = 0$. The physical configuration of the problem as:

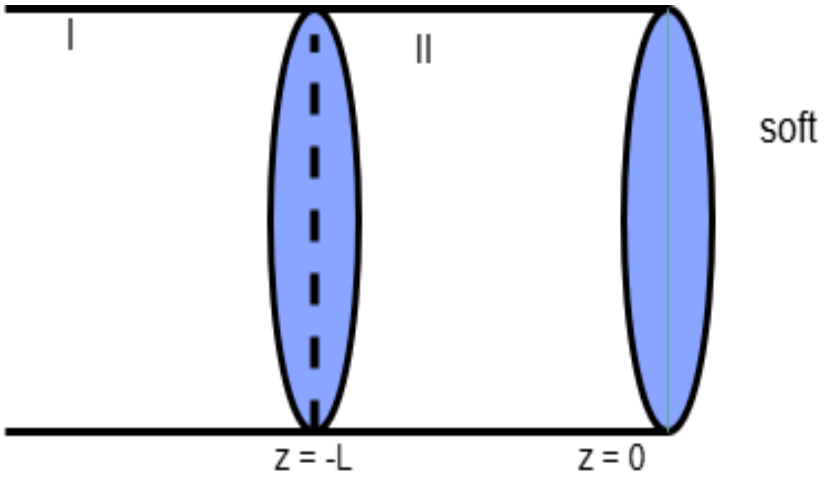

FIGURE 4.3: The physical Configuration of soft cavity.

The governing boundary value problem consists of the Helmholtz equation, rigid boundary conditions, and membrane conditions. In Region II, the non-dimensional form of the Helmholtz equation and the corresponding rigid boundary condition are given as follows:

$$\left\{\frac{\partial^2}{\partial r^2}+\frac{1}{r}\frac{\partial}{\partial r}+\frac{\partial^2}{\partial z^2}+k^2\right\}P_{II}(r,z), \tag{4.38}$$

$$P_{II}(r,0)=0. \tag{4.39}$$

By using (4.6) into (4.39) and get,

$$P_{II}(r,z)=\sum_{n=0}^{\infty}C_n\eta_n R_n(r)+\sum_{n=0}^{\infty}D_n\eta_n R_n(r). \tag{4.40}$$

which implies

$$C_n^a=-D_n^a. \tag{4.41}$$

With soft cavity case, acoustic pressure takes the formulation:

$$P_I^a(r,z)=e^{i\eta_0(z+L)}+\sum_{n=0}^{\infty}B_n^a e^{-i\eta_n(z+L)}R_n(r). \tag{4.42}$$

On using (4.41) into (4.39) we found

$$P^a_{II}(r,z) = 2i\sum_{n=0}^{\infty} C^a_n \sin(s_n z) R_n(r), \tag{4.43}$$

where superscript "a" with variables denotes the soft cavity setting. Note that the quantities B^a_n and C^a_n are amplitudes of soft cavity modes and will be found through the interface conditions.

As we have assumed the membrane interfaces at $z = L$ with soft cavity configuration, the membrane equation substituting (4.14), (4.15), (4.16), and (4.17) into the membrane displacement (solid) (4.18) leading to:

$$\begin{aligned}&\sum_{n=0}^{\infty}\left(-\gamma_n^2 A^a_n + \omega^2\frac{\rho_s}{T}A^a_n + i\omega\frac{R_f}{T}(A^a_n - F^a_n)\right)\xi_n(r)\\ &= -\frac{(1-\Omega)}{T}\left(1 + \sum_{n=0}^{\infty} B^a_n R_{1n}(r) + 2i\sum_{n=0}^{\infty} C^a_n \sin(s_n L) R_{2n}(r)\right).\end{aligned} \tag{4.44}$$

On multiplying (4.44) by $r\xi_m(r)$ and integrating from 0 to a it is found that

$$\begin{aligned}&\sum_{n=0}^{\infty}\left((-\gamma_n^2 A^a_n + \omega^2\frac{\rho_s}{T}A^a_n + i\omega\frac{R_f}{T}(A^a_n - F^a_n)\right)\int_0^a \xi_n(r)\xi_m(r) r dr\\ &= -\frac{(1-\Omega)}{T}\left(1 + \sum_{n=0}^{\infty} B^a_n + 2i\sum_{n=0}^{\infty} C^a_n \sin(s_n L)\right)\int_0^a R_n(r)\xi_m(r) r dr.\end{aligned} \tag{4.45}$$

On using orthogonality relation, (4.45) gives

$$\begin{aligned}&\left(-\lambda_n^2 A^a_m + \omega^2\frac{\rho_s}{T}A^a_m + i\omega\frac{R_f}{T}(A^a_m - F^a_m)\right)\\ &= -\frac{(1-\Omega)}{T E^a_m}\left(L_{n0} + \sum_{n=0}^{\infty} B^a_n + 2\sum_{n=0}^{\infty} C^a_n \sin(s_n L) L_{nm}\right),\end{aligned} \tag{4.46}$$

where

$$L_{n0} = \int_0^a \xi_m(r) r dr,$$

$$L_{nm} = \int_0^a R_n(r)\xi_m(r) r dr.$$

By substituting (4.14), (4.15), (4.16), and (4.17) into the membrane displacement (fluid) (4.19) and we get:

$$\begin{aligned}&\sum_{n=0}^{\infty}\Big(-\omega^2\rho_0\Omega h F_n^a+i\omega R_f(A_n^a-F_n^a)\Big)\xi_n(r)\\&=\Omega\big(1+\sum_{n=0}^{\infty}B_n^a+2i\sum_{n=0}^{\infty}C_n^a\sin(s_nL)\big)R_n(r).\end{aligned}\tag{4.47}$$

Multiplying (4.47) with $r\xi_m(r)$ and integrating $0\le r\le a$ we get

$$\begin{aligned}&\sum_{n=0}^{\infty}\Big(-\omega^2\rho_0\Omega h F_n^a+i\omega R_f(A_n^a-F_n^a)\Big)\int_0^a\xi_n(r)\xi_m(r)rdr\\&=\Omega\big(1+\sum_{n=0}^{\infty}B_n+2i\sum_{n=0}^{\infty}C_n\sin(s_nL)\big)\int_0^a R_n(r)\xi_m(r)rdr.\end{aligned}\tag{4.48}$$

On using orthogonality relation, (4.48) gives

$$\begin{aligned}&\Big(-\omega^2\rho_0\Omega h F_m^a+i\omega R_f(A_m^a-F_m^a)\Big)\\&=\frac{\Omega}{E_m}\Big(L_{n0}+\sum_{n=0}^{\infty}B_n^a+2\sum_{n=0}^{\infty}C_n^a\sin(s_nL)L_{nm}\Big),\end{aligned}\tag{4.49}$$

where

$$L_{no}=\int_0^a\xi_m(r)rdr,$$

and

$$L_{nm}=\int_0^a R_n(r)\xi_m(r)rdr.$$

By simplification (4.14), (4.15), (4.16), and (4.17) into (4.20) and after some arrangement we found;

$$\frac{i}{\omega^2\rho_0}\Big(\eta_0-\sum_{n=0}^{\infty}B_n^a\eta_n R_n(r)\Big)=\sum_{n=0}^{\infty}\Big((1-\Omega)A_n^a-(\Omega)B_n^a\Big)\xi_n(r).\tag{4.50}$$

Multiplying (4.50) with $rR_m(r)$ and integrating $0\le r\le a$ and we get

$$\begin{aligned}&\frac{i}{\omega^2\rho_0}\Big(\eta_0\int_0^a R_m(r)rdr-\sum_{n=0}^{\infty}B_n^a\eta_n\int_0^a R_n(r)R_m(r)rdr\Big)\\&=\Big((1-\Omega)A_n^a-\Omega B_n^a\Big)\int_0^a\xi_n(r)R_m(r)rdr.\end{aligned}\tag{4.51}$$

On using orthogonality relation, (4.51) gives

$$\frac{i}{\omega^2\rho_0}\left(\eta_0\delta_{n0} - B_m^a\eta_m G_m\right) = \sum_{n=0}^{\infty}\left((1-\Omega)A_n^a - \Omega B_n^a\right)L_{nm}. \tag{4.52}$$

By simplification (4.14),(4.15),(4.16) and (4.17) into the continuity of velocity in membrane (4.21) we found;

$$\frac{2i}{\omega^2\rho_0}\sum_{n=0}^{\infty} s_n C_n^a \cos(s_n L)R_n(r) = \sum_{n=0}^{\infty}\left((1-\Omega)A_n^a - (\Omega)B_n^a\right)\xi_n(r). \tag{4.53}$$

Multiplying (4.53) with $rR_m(r)$ and integrating $0 \le r \le a$ we get

$$\begin{aligned}&\frac{2i}{\omega^2\rho_0}\sum_{n=0}^{\infty} s_n^a C_n^a \cos(s_n L)\int_0^a R_n(r)R_m(r)rdr\\ &= \sum_{n=0}^{n\infty}\left((1-\Omega)A_n^a - (\Omega)B_n^a\right)\int_0^a \xi_n(r)R_m(r)rdr.\end{aligned} \tag{4.54}$$

By using orthogonality relation on (4.54) and found,

$$\frac{2is_m}{\omega^2\rho_0}C_m^a\cos(s_m L) = \frac{i\omega}{G_m}\sum_{n=0}^{n\infty}\left((1-\Omega)A_n^a - \Omega B_n^a\right)L_{nm}. \tag{4.55}$$

By invoking (4.14), (4.15), (4.16) and (4.17), into the normal velocity (4.22) the resulting equation is

$$i\left(\eta_0 - \sum_{n=0}^{\infty} B_n^a\eta_n R_n(r)\right) = 2i\sum_{n=0}^{\infty} s_n C_n^a\cos(s_n L)R_n(r). \tag{4.56}$$

Multiplying (4.56) and with $rR_m(r)$ and integrating $0 \le r \le a$, we obtain

$$\begin{aligned}&i\left(\eta_0\int_0^a R_m(r)rdr - \sum_{n=0}^{\infty} B_n^a\eta_n\int_0^a R_n(r)R_m(r)rdr\right)\\ &= 2i\sum_{n=0}^{\infty} s_n C_n^a\cos(s_n L)\int_0^a R_n(r)R_m(r)rdr.\end{aligned} \tag{4.57}$$

Applying orthogonality relation, (4.57) gives

$$i(G_m\eta_0\delta_{n0} - B_m^a\eta_m G_m) = 2is_m C_m^a\cos(s_m L)G_m. \tag{4.58}$$

After simplification

$$B_m^a = \frac{1}{\eta_m}\{\eta_0\delta_{n0} - 2s_nC_n^a\cos(s_mL)\}, \tag{4.59}$$

where

$$\delta_{n0} = \int_0^a R_m(r)rdr.$$

4.4 Numerical Results and Discussion

The symmetric and anti-symmetric problems are solved numerically by truncating the equations to N terms. This truncation is necessary to obtain a finite number of equations that can be solved using numerical methods.

The resulting systems of equations are then solved using MATHEMATICA's "NSolve" function, which is a powerful tool for solving systems of nonlinear equations. To obtain numerical solutions, specific values are assigned to the various parameters in the equations, as listed in reference a, surface density ρ_s, tension T_0, damping coefficient η, angular frequency Ω, fluid resistance R_f, thickness h, length L, and frequency f.

The chosen values are as follows: $a = 0.05$ m (radius), $\rho_s = 0.174$ kg/m^2 (surface density), $T_0 = 85$ N/m (tension), $\eta = 0.005$ (damping coefficient), $\Omega = 0.0018$, $R_f = 0.15$ Rayls (fluid resistance), $h = 0.2$ mm (thickness), $L = 0.1$ m (length), and $f = 1000$ Hz (frequency). These values are chosen to represent a specific physical system, and the numerical solutions obtained using these values can be used to gain insight into the behavior of this system. For the numerical solution, the equations are truncated to 10 terms. This truncation is sufficient to capture the important dynamics of the system, while also keeping the computational cost reasonable.

In Figs. 4.4-4.9, the results for the symmetric problem are displayed. The real and imaginary parts of normal velocities are shown against radius r at at $z = -L$ in Figs. 4.4 and 4.5. Both velocity components coincide which validates the truncated solution at given numerical values of parameters. In Figs. 4.6 and 4.14, the real parts of normal velocity $\phi_{2z}(r, z)$ are shown against radius r at $z = 0$ Hz. It can be seen that both components are zero as considered in symmetric setting of the problem. But the pressure at the is not zero which can be seen in Figs. 4.8 and 4.9.

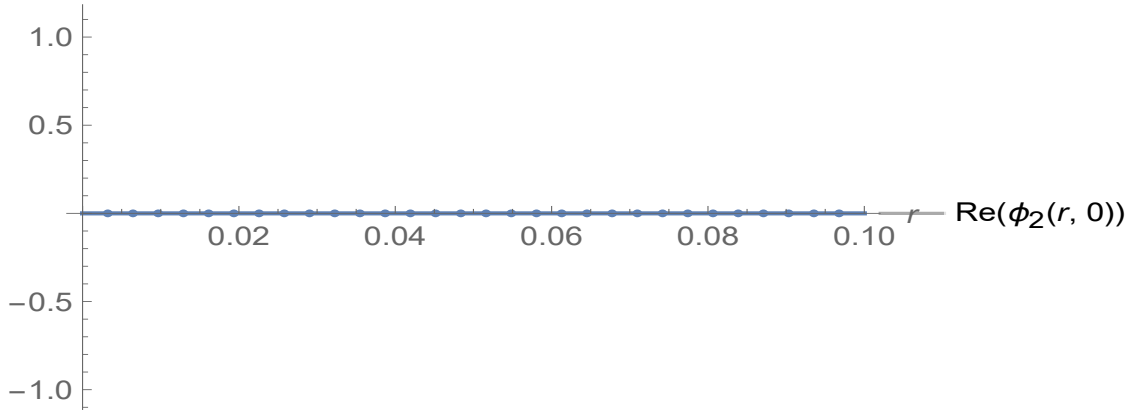

FIGURE 4.4: For symmetric case, the real parts of the velocities against r at $z = -L$

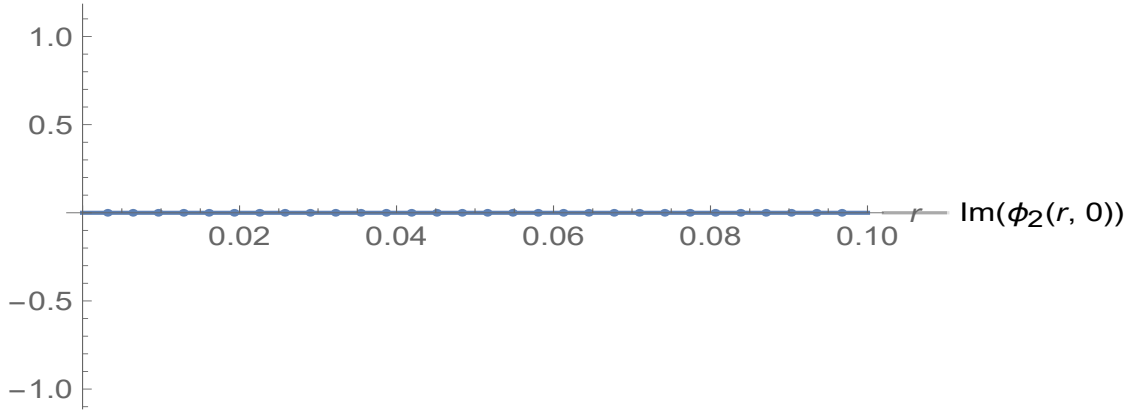

FIGURE 4.5: For symmetric case, the imaginary parts of the velocities against r at $z = -L$.

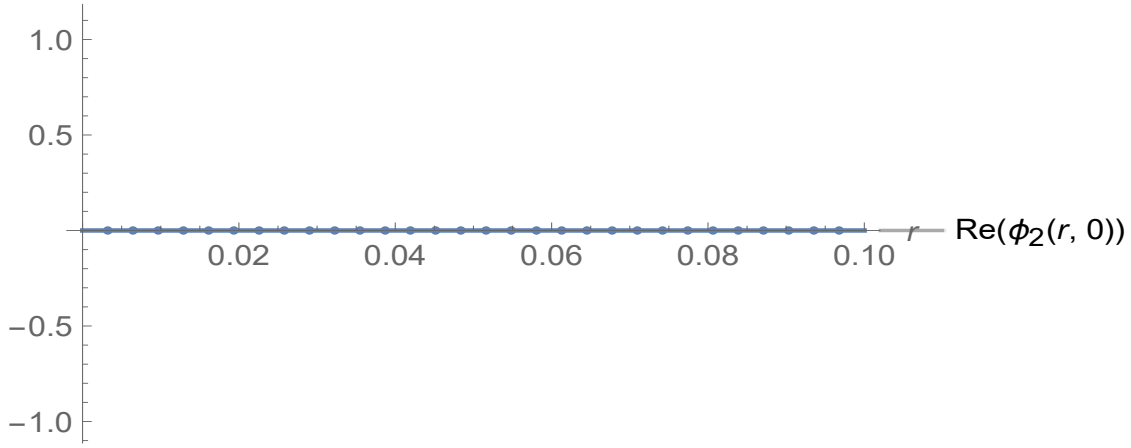

FIGURE 4.6: For symmetric case, the real parts of the velocity $\phi_{2z}(r, z)$ against r at $z = 0$

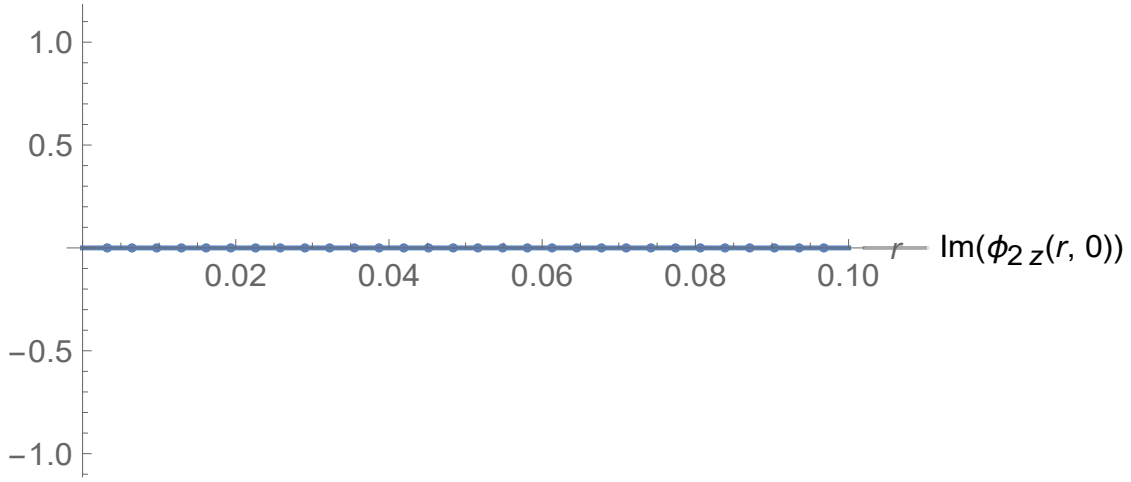

FIGURE 4.7: For symmetric case, the imaginary parts of the velocity $\phi_{2z}(r, z)$ against r at $z = 0$.

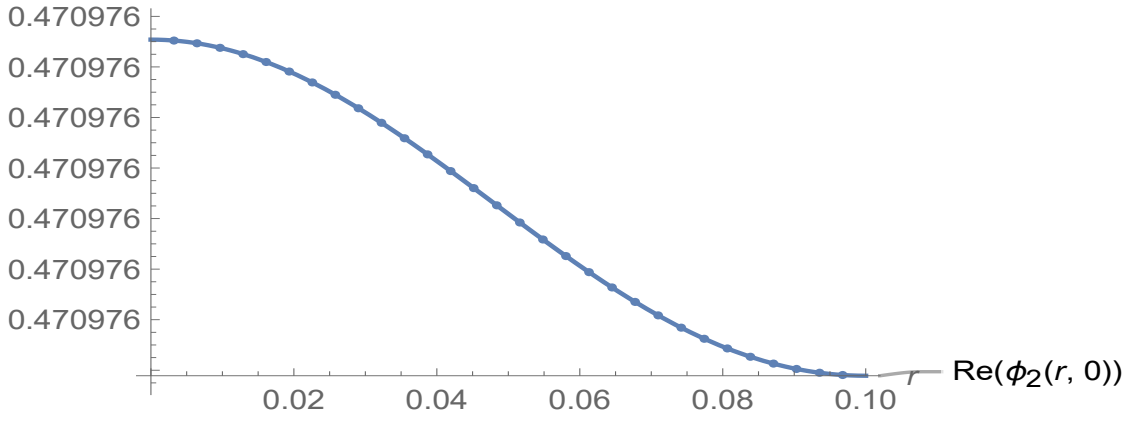

FIGURE 4.8: For symmetric case, the real parts of the pressure $\phi_2(r, z)$ against r at $z = 0$

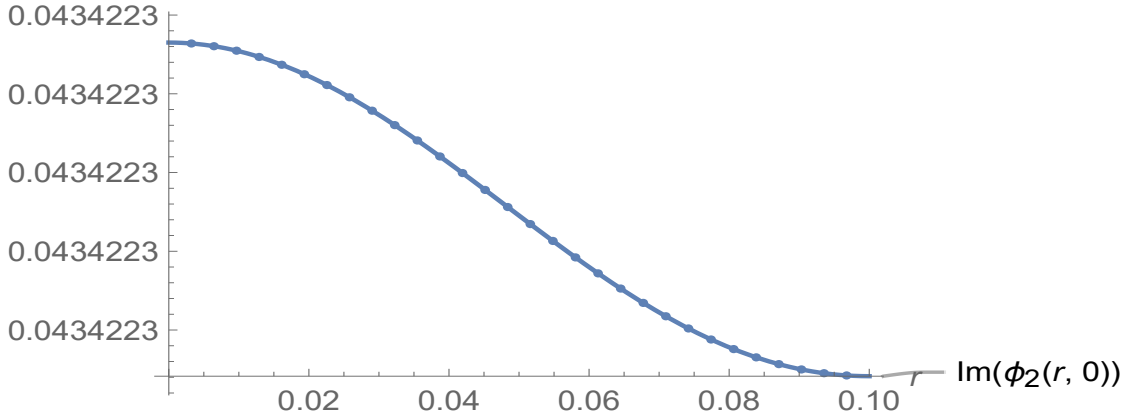

FIGURE 4.9: For symmetric case, the imaginary parts of the pressure $\phi_2(r, z)$ against r at $z = 0$.

In Figs. 4.10-4.17, the results for the anti-symmetric problem are displayed. The real and imaginary parts of normal velocities are shown against radius r at $z = -L$ in Figs. 4.10 and 4.11. Both velocity components coincide which validates the truncated solution at given numerical values of parameters. In Figs. 4.12 and 4.15, the real parts of pressure $\phi_2(r, z)$ are shown against radius r at $z = 0$ Hz. It can be seen that both components are zero as considered in anti-symmetric setting of the problem. But the the velocity components at $z = 0$ are not zero which can be seen in Figs. 4.16 and 4.17.

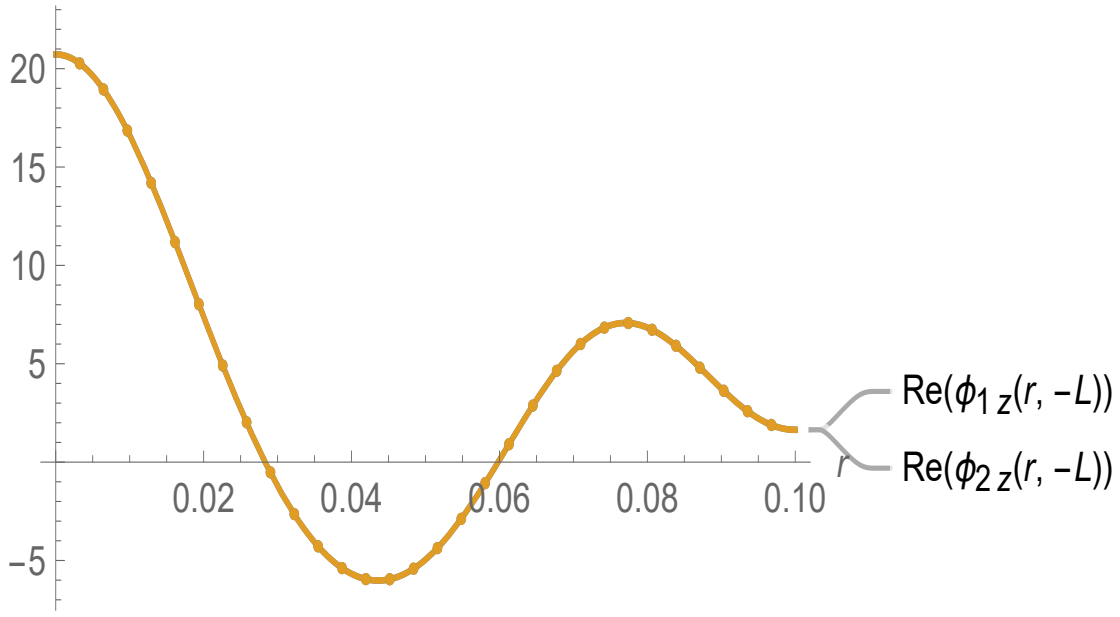

FIGURE 4.10: For anti-symmetric case, the real parts of the velocities against r at $z = -L$

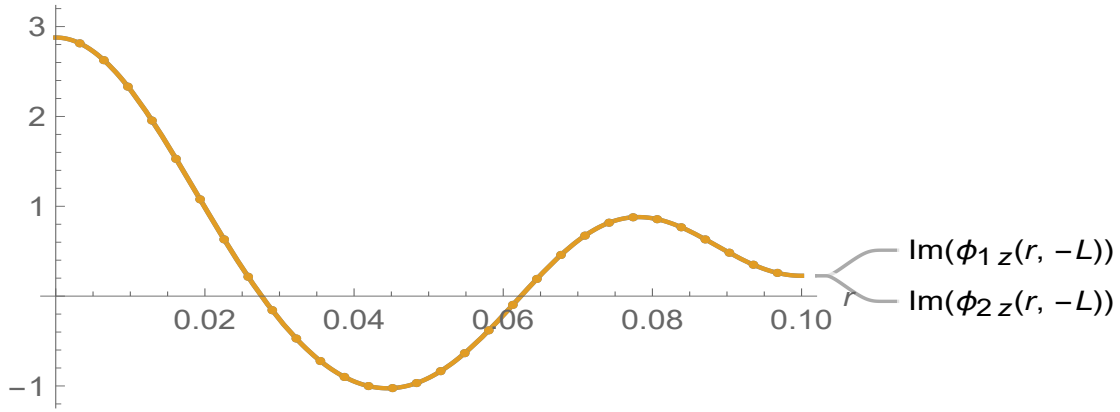

FIGURE 4.11: For anti-symmetric case, the imaginary parts of the velocities against r at $z = -L$.

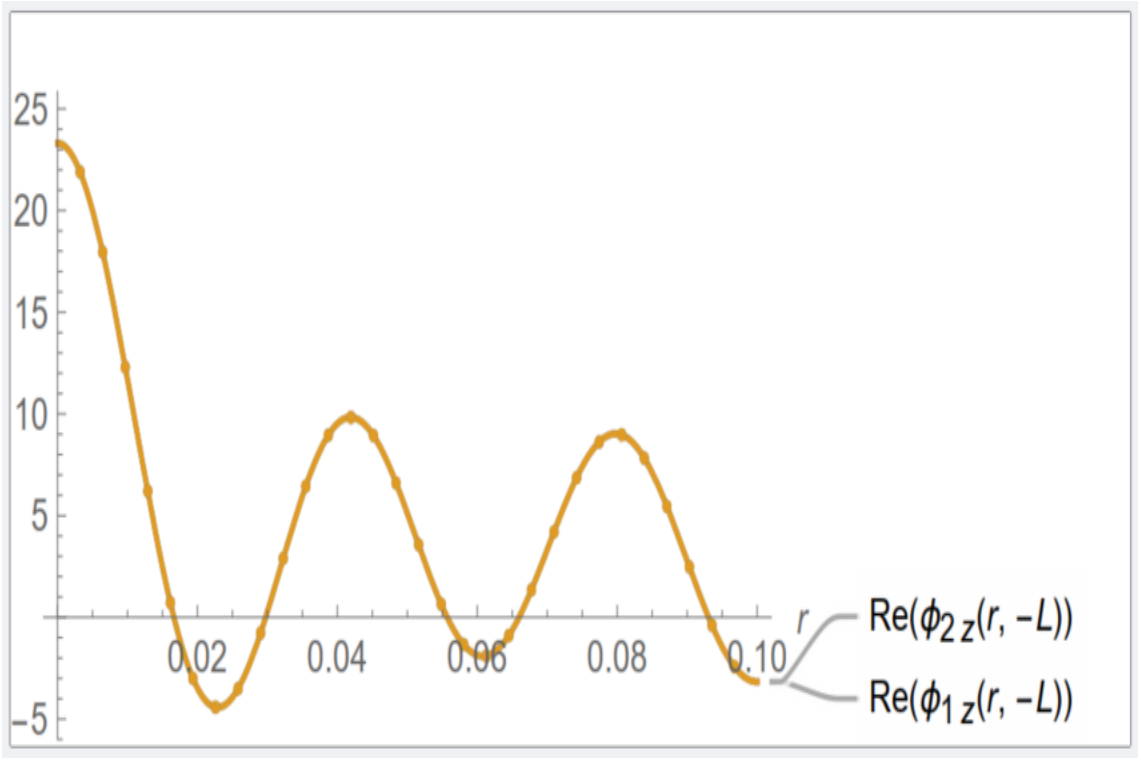

FIGURE 4.12: For anti-symmetric case, the real parts of the pressure $\phi_{2z}(r, z)$ against r at $z = 0$

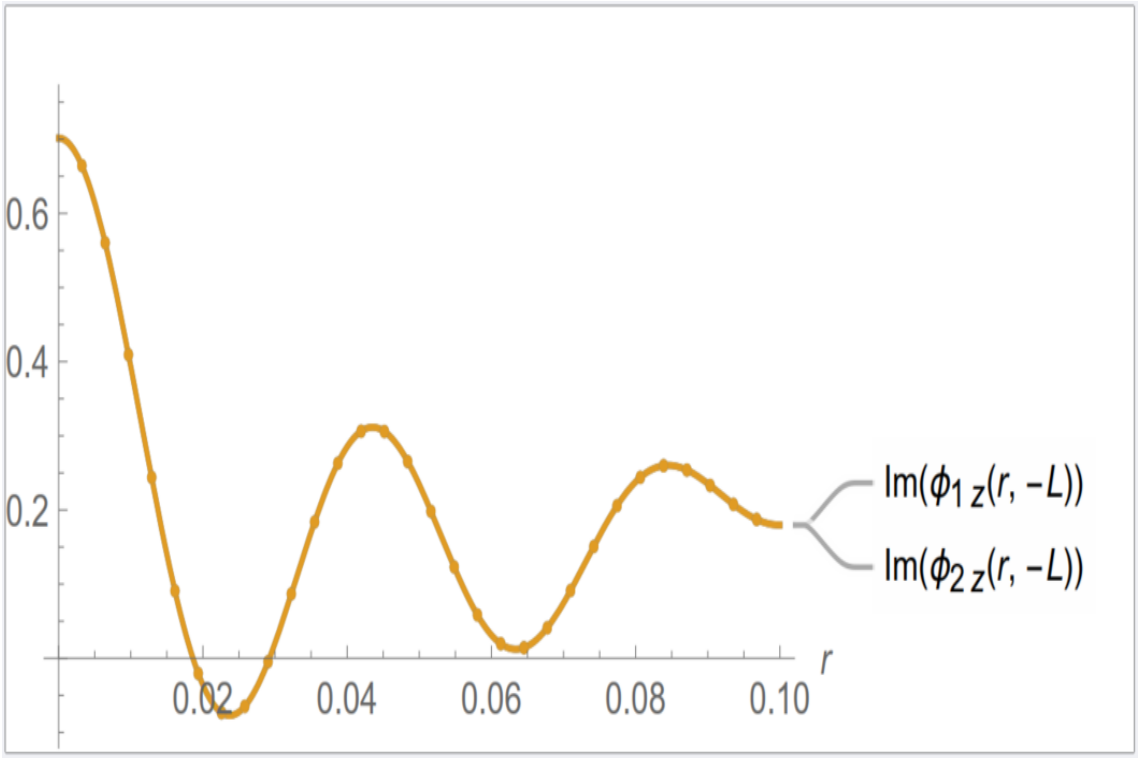

FIGURE 4.13: For symmetric case, the imaginary parts of the velocity $\phi_{2z}(r, z)$ against r at $z = 0$.

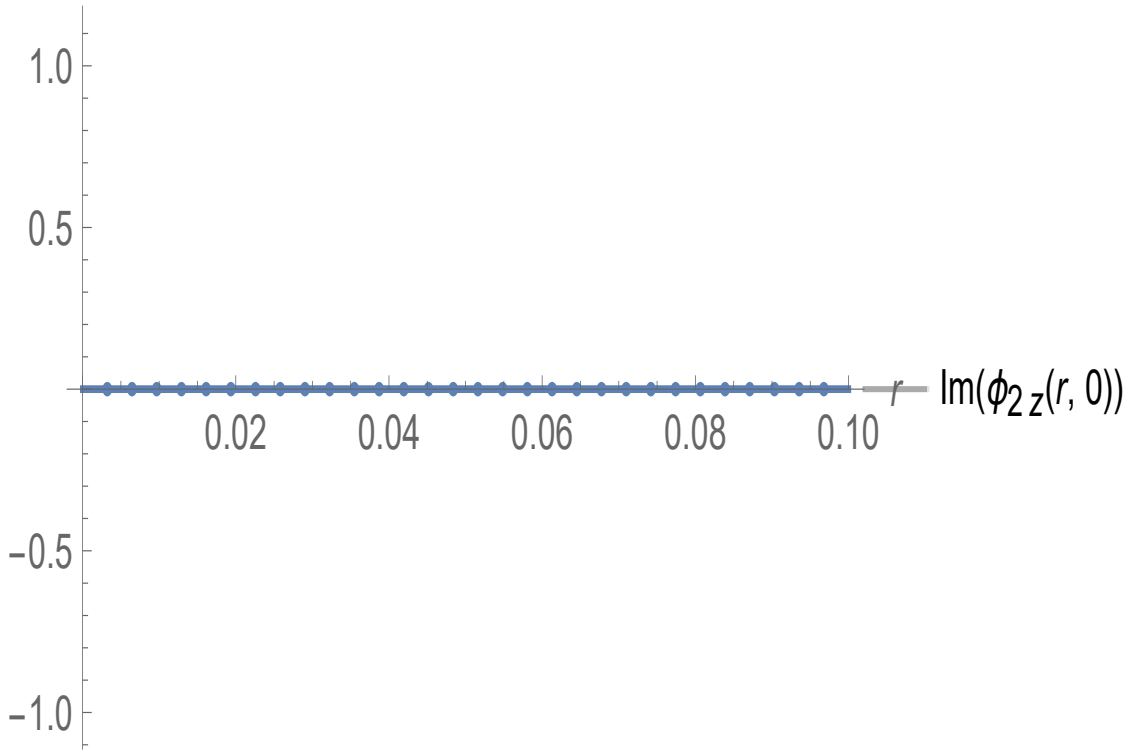

FIGURE 4.14: For symmetric case, the imaginary parts of the velocity $\phi_{2z}(r, z)$ against r at $z = 0$.

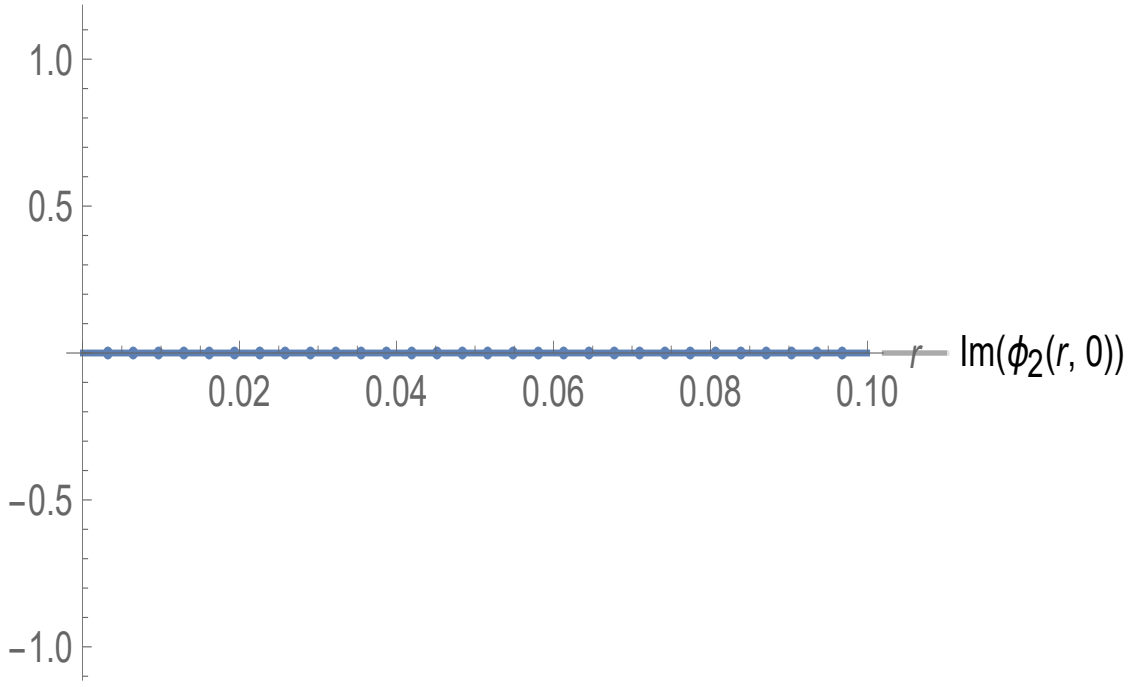

FIGURE 4.15: For anti-symmetric case, the imaginary parts of the pressure $\phi_2(r, z)$ against r at $z = 0$.

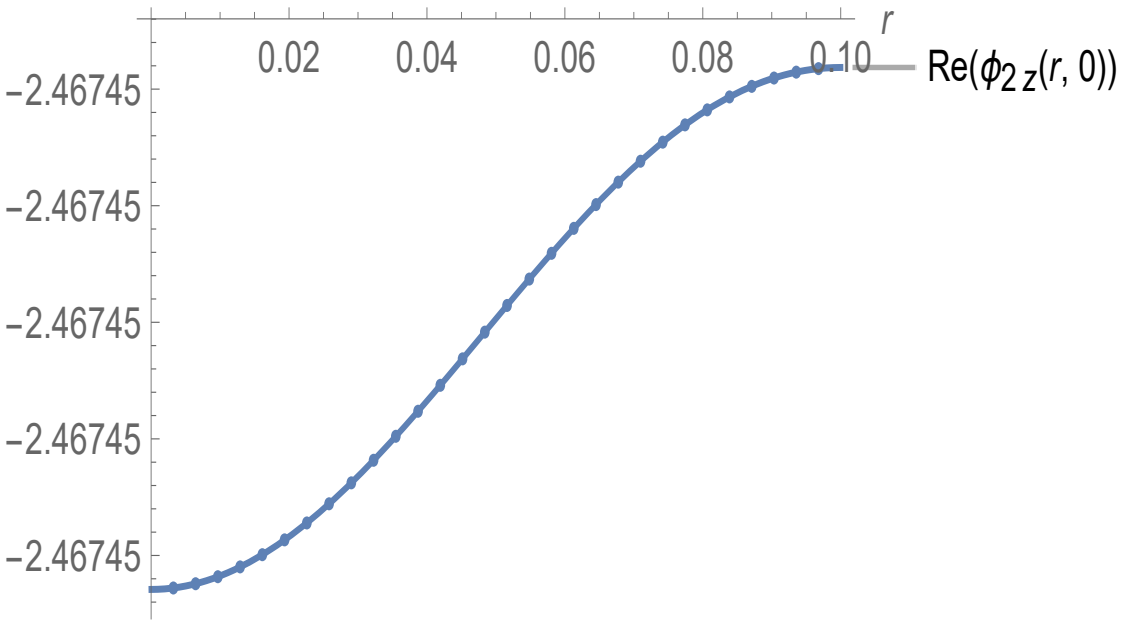

FIGURE 4.16: For symmetric case, the real parts of the velocity $\phi_{2z}(r, z)$ against r at $z = 0$

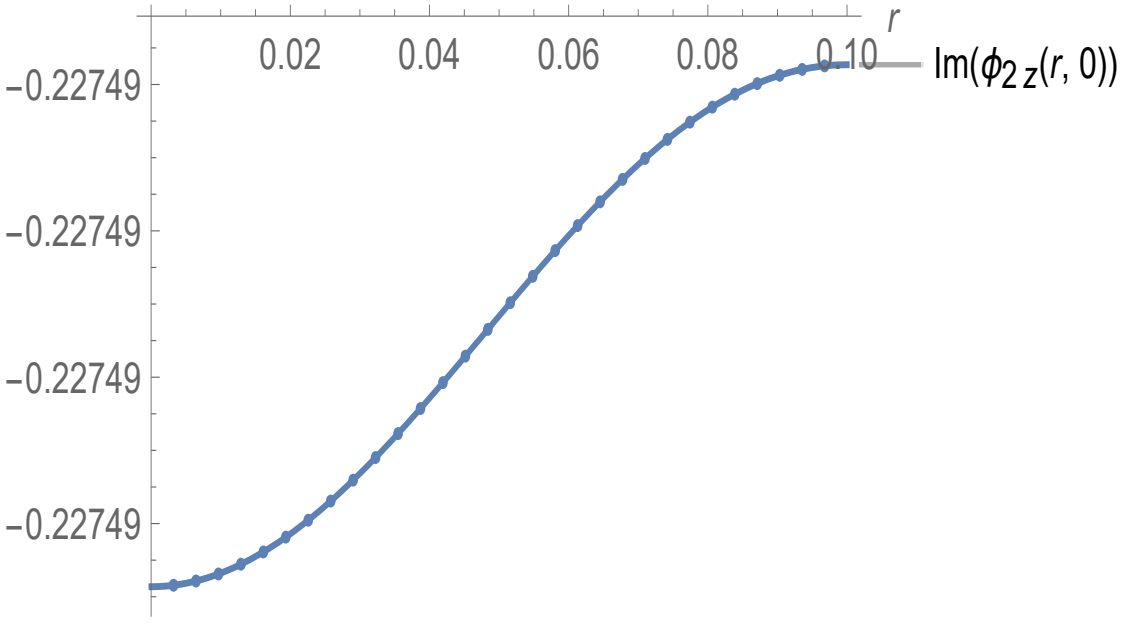

FIGURE 4.17: For anti-symmetric case, the imaginary parts of the velocity $\phi_{2z}(r, z)$ against r at $z = 0$.

The numerical results obtained for both symmetric and anti-symmetric problems demonstrate the validity and accuracy of the truncated solution. The coincidence

of velocity components at $z = -L$ for both problems confirms that the truncated solution captures the essential dynamics of the system. Furthermore, the results at $z = 0$ show that the solution satisfies the symmetry conditions, with zero velocity components for the symmetric problem and zero pressure components for the anti-symmetric problem. The results also highlight the importance of considering both symmetric and anti-symmetric components in the analysis of the fluid-structure interaction problem. The non-zero pressure at the interface for the symmetric problem and the non-zero velocity components at $z = 0$ for the anti-symmetric problem demonstrate the complex dynamics of the system.

Chapter 5

Summary and Conclusion

This research has presented a comprehensive study on the reflection and transmission of acoustic waves in cylindrical waveguides incorporating membrane interfaces. The theoretical framework developed in this study provides valuable insights into the propagation and scattering of acoustic waves when interacting with permeable membranes. By employing the mode-matching technique, the study effectively addresses the challenges associated with modeling complex acoustic environments.

In the permeable circular membrane is assumed in a cylindrical waveguide. The fundamental mode radiation is made incident on the permeable membrane which scatter on the interaction with the membrane. The mode matching solution is applied to solve the boundary value problem governing the boundary. The truncated system is solution after trunction which yields the structure and find mode propagation. Increasing the frequency excites additional mode. The presence of additional modes at higher frequency highlight importance of considering the effects of frequency on the dynamics of the system.

In chapter 4, the problem considering permeable membrane backed by rigid cavity and soft cavity are considered. The modeling and solution for symmetric and anti symmetric mode problems are discussed analytically. The findings demonstrate that the frequency esence of tensioned, permeable membranes significantly influences wave behavior, affecting both transmission and reflection properties. The study examined

different configurations, including rigid and soft cavities, revealing the crucial role of boundary conditions in shaping wave interactions.

The implications of this work extend to various engineering applications, including noise control, architectural acoustics, and industrial sound management. The developed models can aid in designing more efficient noise barriers, acoustic filters, and resonators tailored to specific requirements. Future research could focus on experimental validation of the theoretical predictions, exploring more complex geometries and multi-layered membrane structures to further refine the modeling approach.

In summary, this study contributes to the understanding of acoustical wave interactions with tensioned, permeable membranes, providing a solid foundation for future advancements in noise control engineering and related fields.

Bibliography

[1] J. Ma, D. Ping, and X. Dong. Recent developments of graphene oxide-based membranes: a review. *Membranes*, 7(3):52, 2017.

[2] X. Sun, S. Ma, L. Han, R. Li, U. Schlick, P. Chen, and G. Huang. The effect of a semi-permeable membrane-covered composting system on greenhouse gas and ammonia emissions in the tibetan plateau. *Journal of Cleaner Production*, 204: 778–787, 2018.

[3] M. Toyoda, K. Funahashi, T. Okuzono, and K. Sakagami. Predicted absorption performance of cylindrical and rectangular permeable membrane space sound absorbers using the three-dimensional boundary element method. *Sustainability*, 11(9):2714, 2019.

[4] A. Hao, X. Wan, X. Liu, R. Yu, and J. Shui. Inorganic microporous membranes for hydrogen separation: Challenges and solutions. *Nano Research Energy*, 1(2), 2022.

[5] H. Wang, S. Zhao, Y. Liu, R. Yao, X. Wang, Y. Cao, D. Ma, M. Zou, A. Cao, X. Feng, et al. Membrane adsorbers with ultrahigh metal-organic framework loading for high flux separations. *Nature Communications*, 10(1):4204, 2019.

[6] J. W. Strutt and J. W. S. Rayleigh. *The theory of sound*, volume 1. Macmillan, 1877.

[7] S. Kirkup. The boundary element method in acoustics: A survey. *Applied Sciences*, 9(8):1642, 2019.

[8] C. M. Mak and Z. Wang. Recent advances in building acoustics: An overview of prediction methods and their applications. *Building and Environment*, 91: 118–126, 2015.

[9] C. Zhang, H. Li, J. Gong, J. Chen, Z. Li, Q. Li, M. Cheng, X. Li, and J. Zhang. The review of fiber-based sound-absorbing structures. *Textile Research Journal*, 93(1-2):434–449, 2023.

[10] A. D. Pierce. Reflection, transmission, and excitation of plane waves. *Acoustics: an introduction to its physical principles and applications*, pages 115–175, 2019.

[11] C. F. de Lannoy, E. Soyer, and M. R. Wiesner. Optimizing carbon nanotube-reinforced polysulfone ultrafiltration membranes through carboxylic acid functionalization. *Journal of membrane science*, 447:395–402, 2013.

[12] Z. Mo, G. Song, T. Shi, and J. S. Bolton. The impact of boundary conditions on the acoustical behavior of lightweight granular particle stacks. In *INTER-NOISE and NOISE-CON Congress and Conference Proceedings*, volume 270, pages 6252–6258. Institute of Noise Control Engineering, 2024.

[13] Y.-T. Wang and R. Craster. Designing hyper-thin acoustic metasurfaces with membrane resonators. *arXiv preprint arXiv:2007.09759*, 2020.

[14] A. McAlpine and M. J. Fisher. On the prediction of "buzz-saw" noise in acoustically lined aero-engine inlet ducts. *Journal of Sound and Vibration*, 265(1): 175–200, 2003.

[15] D. Takahashi, K. Sakagami, and M. Morimoto. Acoustic properties of permeable membranes. *The Journal of the Acoustical Society of America*, 99(5):3003–3009, 1996.

[16] M. Afzal, N. Ahmed, M. Safdar, and M. Umar. On the modeling of sound sources in waveguides with structural variations and sound-absorbent materials. *Communication in Nonlinear Science and Numerical Simulation*, 145:108714, 2025.

[17] H. Bilal and M. Afzal. Application of the matrix element method: A mode-matching approach for wave-bearing cavities in complex media. *Chaos, Solitons Fractals*, 189:115589, 2024.

[18] S. Rizvi and M. Afzal. Electromagnetic wave scattering in plasma beam-driven waveguides under strong magnetic fields. *Communications in Theoretical Physics*, 76:115502, 2024.

[19] M. Afzal and T. Nawaz. Trifurcated lined ducts: A comprehensive study on noise reduction strategies. *PLoS ONE*, 19(7):e0306115, 2024. doi: 10.1371/journal.pone.0306115. URL https://doi.org/10.1371/journal.pone.0306115.

[20] M. Afzal, T. Aziz, and H. M. S. Bahaidarah. Dynamical behavior of fluid–structure interaction in ducts with rigid and flexible interfaces: Modeling and analysis. *Partial Differential Equations in Applied Mathematics*, 11:100789, 2024. doi: 10.1016/j.padiff.2024.100789. URL https://doi.org/10.1016/j.padiff.2024.100789.

[21] S. Shafique, M. A. Ahmad, and M. Afzal. Optimizing the noise control in a two-layer conduit. *Physica Scripta*, 99:065227, 2024. doi: 10.1088/1402-4896/ad451e.

[22] M. Afzal, M. Safdar, and H. N. Alahmadi. Analyzing the impact of flexible shells and sound absorbent lining on acoustic wave behavior in ducts. *Mathematical Methods in the Applied Science*, 2024. doi: 10.1002/mma.10133. URL https://doi.org/10.1002/mma.10133.

[23] S. Shafique, A. Ahmad, and M. Afzal. Optimizing the noise control in a two-layer conduit. *Physica Scripta*, 99(6):065227, 2024.

[24] S. Rizvi and M. Afzal. Cold plasma-induced effects on electromagnetic wave scattering in waveguides: a mode-matching analysis. *Communications in Theoretical Physics*, 76(3):035501, 2024.

[25] A. D. Alruwaili, M. Afzal, H. N. Alahmadi, and A. Wahab. Wave scattering in cylindrical waveguides: Analyzing flexible shells and liner conditions. *Alexandria Engineering Journal*, 91:610–619, 2024.

[26] A. D. Alruwaili, M. Afzal, M. Tanveer, and H. N. Alahmadi. Analyzing monopole sources modeling with structural variations and material contrast: An analytical perspective. *Chaos, Solitons Fractals*, 179(1):114434, 2024.

[27] P. M. Morse and K. U. Ingard. *Theoretical acoustics*. Princeton University Press, 1986.

[28] L. Cao, Q. Fu, Y. Si, B. Ding, and J. Yu. Porous materials for sound absorption. *Composites Communications*, 10:25–35, 2018.

[29] J. Allard and N. Atalla. *Propagation of sound in porous media: modelling sound absorbing materials*. John Wiley & Sons, 2009.

[30] Y. Kang, Y. Yang, L.-C. Yin, X. Kang, G. Liu, and H.-M. Cheng. An amorphous carbon nitride photocatalyst with greatly extended visible-light-responsive range for photocatalytic hydrogen generation. *Advanced Materials*, 27(31):4572–4577, 2015.

[31] Y. J. Kang and J. S. Bolton. A finite element model for sound transmission through foam-lined double-panel structures. *The Journal of the Acoustical Society of America*, 99(5):2755–2765, 1996.

[32] J. Song. *Nonfibrous sound-absorbing materials*. PhD thesis, Purdue University, 2003.

[33] E. J. Brambley and N. Peake. Classification of aeroacoustically relevant surface modes in cylindrical lined ducts. *Wave Motion*, 43(4):301–310, 2006.

[34] X. Wang and C. M. Mak. Wave propagation in a duct with a periodic helmholtz resonators array. *The Journal of the Acoustical Society of America*, 131(2):1172–1182, 2012.

[35] A. Abbas, M. B. Jeelani, A. S. Alnahdi, and A. Ilyas. Mhd williamson nanofluid fluid flow and heat transfer past a non-linear stretching sheet implanted in a porous medium: effects of heat generation and viscous dissipation. *Processes*, 10 (6):1221, 2022.

[36] J. B. Lawrie and I. D. Abrahams. An orthogonality relation for a class of problems with high-order boundary conditions; applications in sound-structure interaction. *The Quarterly Journal of Mechanics and Applied Mathematics*, 52(2):161–181, 1999.

[37] M. Afzal, T. Nawaz, and R. Nawaz. Scattering characteristics of planar trifurcated waveguide structure containing multiple discontinuities. *Waves in Random and Complex Media*, 2020. doi: 10.1080/17455030.2020.1864062.

[38] S. Shafique, M. Afzal, and R. Nawaz. On the attenuation of fluid–structure coupled modes in a nonplanar waveguide. *Mathematics and Mechanics of Solids*, 25(10):1831–1850, 2020. doi: 10.1177/1081286520929047.

[39] M. Afzal and S. Shafique. Attenuation analysis of flexural modes with absorbent lined flanges and different edge conditions. *Journal of the Acoustical Society of America*, 148(1):85–99, 2020. doi: 10.1121/10.0001534.

[40] M. Afzal, J. U. Satti, and R. Nawaz. Scattering characteristics of nonplanar trifurcated waveguides. *Meccanica*, 55:977–988, 2020. doi: 10.1007/s11012-019-01115-4.

[41] J. U. Satti, M. Afzal, and R. Nawaz. Scattering analysis of a partitioned wave-bearing cavity containing different material properties. *Physica Scripta*, 94: 115223, 2019. doi: 10.1088/1402-4896/ab1c94.

[42] T. Nawaz, M. Afzal, and R. Nawaz. The scattering analysis of trifurcated waveguide involving structural discontinuities. *Advances in Mechanical Engineering*, 11(7):1–10, 2019. doi: 10.1177/1687814019856078.

[43] H. Bilal and M. Afzal. Acoustic wave scattering from a wave-bearing cavity in a rectangular waveguide. *Journal of the Acoustical Society of America*, 144:1681, 2018. doi: 10.1121/1.5055302.

[44] A. Ullah, R. Nawaz, and M. Afzal. Fluid-structure coupled wave scattering in a flexible duct at the junction of planar discontinuities. *Advances in Mechanical Engineering*, 9(7):1–11, 2017. doi: 10.1177/1687814017711344.

[45] J. B. Lawrie and M. Afzal. Acoustic scattering in a waveguide with a height discontinuity bridged by a membrane: a tailored galerkin approach. *Journal of Engineering Mathematics*, 105(1):99–115, 2017. doi: 10.1007/s10665-017-9905-1.

[46] S. Shafique, M. Afzal, and R. Nawaz. On mode matching analysis of fluid-structure coupled wave scattering between two flexible waveguides. *Canadian Journal of Physics*, 95(6):581–589, 2017. doi: 10.1139/cjp-2016-0687.

[47] M. Afzal, R. Nawaz, and A. Ullah. Attenuation of dissipative device involving coupled wave scattering. *Applied Mathematics and Computation*, 290(1):154–163, 2016. doi: 10.1016/j.amc.2016.06.016.

[48] R. Nawaz, M. Afzal, and M. Ayub. Acoustic propagation in two-dimensional waveguide for membrane bounded ducts. *Communications in Nonlinear Science and Numerical Simulation*, 20(2):421–433, 2015. doi: 10.1016/j.cnsns.2014.05.020.

[49] R. Huang and D. Zhang. Application of mode matching method to analysis of axisymmetric coaxial discontinuity structures used in permeability and/or permittivity measurement. *Progress In Electromagnetics Research*, 67:205–230, 2007.

[50] M. Afzal, M. Ayub, R. Nawaz, and A. Wahab. Mode-matching solution of a scattering problem in flexible waveguide with abrupt geometric changes. *Imaging, Multi-scale and High Contrast Partial Differential Equations, American Mathematic Society*, 660:113–129, 2016.

[51] M. H. Meylan and A. Bashir. Mode matching analysis for wave scattering in triple and pentafurcated spaced ducts. *Mathematical Methods in the Applied Sciences*, 39(11):3043–3057, 2016.

[52] M. Afzal and M. Safdar. Mode-matching technique for analyzing scattering in elastic shell chambers: Applications in trifurcated waveguide systems. *Communication in Nonlinear Science and Numerical Simulation*, 130:107723, 2023. doi: 10.1016/j.cnsns.2023.107723.

[53] H. Bilal, M. U. Khan, and M. Afzal. Silencing performance of the wave-bearing cavity with porous media. *Journal of Vibration and Control*, 2023. doi: 10.1177/1077546323120938. URL https://doi.org/10.1177/1077546323120938.

[54] M. Afzal, M. O. Alkinidri, M. Safdar, and H. Bilal. On the scattering of cylindrical elastic shell having trifurcation and structural variations at interfaces. *Chaos, Solitons Fractals*, 175:114033, 2023. doi: 10.1016/j.chaos.2023.114033.

[55] M. Afzal, H. Bilal, N. Ahmed, and A. Wahab. Acoustic scattering from a wave-bearing cavity with flexible inlet and outlet. *Mathematical Methods in the Applied Sciences*, 2023. doi: 10.1002/mma.9633. URL https://doi.org/10.1002/mma.9633.

[56] M. Safdar, N. Ahmed, M. Afzal, and A. Wahab. Acoustic scattering in lined panel cavities with membrane interfaces. *Journal of the Acoustical Society of America*, 154:1138–1151, 2023. doi: 10.1121/10.1002/mma.9633.

[57] M. Afzal, N. Akhtar, M. O. Alkinidri, and M. Shutaywi. A mode-matching tailored-galerkin approach for higher order interface conditions and geometric variations. *Mathematics*, 11(3):755, 2023. doi: 10.3390/math11030755.

[58] M. Afzal and H. Bilal. Silencing performance analysis of a membrane cavity with different edge conditions. *Journal of Vibration and Control*, 2022. doi: 10.1177/1077546322111870. URL https://doi.org/10.1177/1077546322111870.

[59] H. Bilal and M. Afzal. Reflection and transmission of acoustic waves through the bridging membrane junctions. *Waves in Random and Complex Media*, 2022. doi: 10.1080/17455030.2022.2051771. URL https://doi.org/10.1080/17455030.2022.2051771.

[60] Bilal and M. Afzal. On the extension of the mode-matching procedure for modeling a wave-bearing cavity. *Mathematics and Mechanics of Solids*, 27(2):348–367, 2022. doi: 10.1177/10812865211054100.

[61] M. Afzal, J. U. Satti, R. Nawaz, and A. Wahab. Scattering analysis of a partitioned membrane-bounded cavity with material contrast. *Journal of the Acoustical Society of America*, 151(1):31–44, 2022. doi: 10.1121/1.5123416.

[62] T. Nawaz, M. Afzal, and A. Wahab. Scattering analysis of a flexible trifurcated lined waveguide structure with step-discontinuities. *Physica Scripta*, 96 (11):115004, 2021. doi: 10.1088/1402-4896/ac0b34.

[63] M. Afzal, S. Shafique, and A. Wahab. Analysis of traveling waveform of flexible waveguides containing absorbent material along flanged junctions. *Communication in Nonlinear Science and Numerical Simulation*, 97:105737, 2021. doi: 10.1016/j.cnsns.2020.105737.

[64] M. Afzal and J. U. Satti. The traveling wave formulation of a splitting chamber containing reactive components. *Archive of Applied Mechanics*, 91:1959–1980, 2021. doi: 10.1007/s00419-020-01822-4.

[65] G. V. Eleftheriades, A. S. Omar, L. P. B. Katehi, and G. M. Rebeiz. Some important properties of waveguide junction generalized scattering matrices in the context of the mode matching technique. *IEEE Transactions on Microwave Theory and Techniques*, 42(10):1896–1903, 1994.

[66] J. S. Bolton and J. Song. Acoustical modeling of tensioned, permeable membranes. 2003.